A&A 599, A142 (2017)
DOI: 10.1051/0004-6361/201629794

Astronomy & Astrophysics

Stellar laboratories

VIII. New Zr IV–VII, Xe IV–V, and Xe VII oscillator strengths and the Al, Zr, and Xe abundances in the hot white dwarfs G191−B2B and RE 0503−289★,★★,★★★

T. Rauch[1], S. Gamrath[2], P. Quinet[2,3], L. Löbling[1], D. Hoyer[1], K. Werner[1], J. W. Kruk[4], and M. Demleitner[5]

1 Institute for Astronomy and Astrophysics, Kepler Center for Astro and Particle Physics, Eberhard Karls University, Sand 1, 72076 Tübingen, Germany
e-mail: rauch@astro.uni-tuebingen.de
2 Physique Atomique et Astrophysique, Université de Mons – UMONS, 7000 Mons, Belgium
3 IPNAS, Université de Liège, Sart Tilman, 4000 Liège, Belgium
4 NASA Goddard Space Flight Center, Greenbelt, MD 20771, USA
5 Astronomisches Rechen-Institut (ARI), Centre for Astronomy of Heidelberg University, Mönchhofstraße 12–14, 69120 Heidelberg, Germany

Received 27 September 2016 / Accepted 6 November 2016

ABSTRACT

Context. For the spectral analysis of high-resolution and high-signal-to-noise spectra of hot stars, state-of-the-art non-local thermodynamic equilibrium (NLTE) model atmospheres are mandatory. These are strongly dependent on the reliability of the atomic data that is used for their calculation.

Aims. To search for zirconium and xenon lines in the ultraviolet (UV) spectra of G191−B2B and RE 0503−289, new Zr IV–VII, Xe IV–V, and Xe VII oscillator strengths were calculated. This allows, for the first time, determination of the Zr abundance in white dwarf (WD) stars and improvement of the Xe abundance determinations.

Methods. We calculated Zr IV–VII, Xe IV–V, and Xe VII oscillator strengths to consider radiative and collisional bound-bound transitions of Zr and Xe in our NLTE stellar-atmosphere models for the analysis of their lines exhibited in UV observations of the hot WDs G191−B2B and RE 0503−289.

Results. We identified one new Zr IV, 14 new Zr V, and ten new Zr VI lines in the spectrum of RE 0503−289. Zr was detected for the first time in a WD. We measured a Zr abundance of -3.5 ± 0.2 (logarithmic mass fraction, approx. 11 500 times solar). We identified five new Xe VI lines and determined a Xe abundance of -3.9 ± 0.2 (approx. 7500 times solar). We determined a preliminary photospheric Al abundance of -4.3 ± 0.2 (solar) in RE 0503−289. In the spectra of G191−B2B, no Zr line was identified. The strongest Zr IV line (1598.948 Å) in our model gave an upper limit of -5.6 ± 0.3 (approx. 100 times solar). No Xe line was identified in the UV spectrum of G191−B2B and we confirmed the previously determined upper limit of -6.8 ± 0.3 (ten times solar).

Conclusions. Precise measurements and calculations of atomic data are a prerequisite for advanced NLTE stellar-atmosphere modeling. Observed Zr IV–VI and Xe VI-VII line profiles in the UV spectrum of RE 0503−289 were simultaneously well reproduced with our newly calculated oscillator strengths.

Key words. atomic data – line: identification – stars: abundances – stars: individual: G191-B2B – stars: individual: RE0503-289 – virtual observatory tools

1. Introduction

The DO-type white dwarf (WD) star RE 0503−289 (WD 0501+527, McCook & Sion 1999a,b), exhibits many lines of the trans-iron elements Zn (atomic number $Z = 30$), Ga (31), Ge (32), As (33), Se (34), Kr (36), Mo (42), Sn (50), Te (52), I (53), Xe (54), and Ba (56) in its ultraviolet spectrum. These were initially identified by Werner et al. (2012b), who determined the Kr and Xe abundances (Sect. 8) based on atomic data available at that time. Calculations of transition probabilities for Zn, Ga, Ge, Kr, Mo, Xe, and Ba in the subsequent years allowed precise abundance measurements for these elements (Rauch et al. 2014a, 2015b, 2012, 2016a, 2014b, 2015a, 2016b, respectively).

Here we report that we have identified lines of an additional element, namely zirconium (40) which has never been detected before in WDs, and calculated new Zr IV–VII transition probabilities to determine its photospheric abundance. To verify the Xe abundance determination of Werner et al. (2012b), we calculated much more complete Xe IV–V and Xe VI transition probabilities.

The hot, hydrogen-rich, DA-type WD G191−B2B (WD 0501+527, McCook & Sion 1999a,b) is a primary flux reference standard for all absolute calibrations from 1000 to

★ Based on observations with the NASA/ESA *Hubble* Space Telescope, obtained at the Space Telescope Science Institute, which is operated by the Association of Universities for Research in Astronomy, Inc., under NASA contract NAS5-26666.

★★ Based on observations made with the NASA-CNES-CSA Far Ultraviolet Spectroscopic Explorer.

★★★ Tables A.9–A.12 and B.5–B.7 are only available via the German Astrophysical Virtual Observatory (GAVO) service TOSS (http://dc.g-vo.org/TOSS).

Table 1. Column densities (in $\mathrm{cm^{-2}}$) and radial velocities (in $\mathrm{km\,s^{-1}}$) used to model interstellar clouds in the line of sight toward RE 0503−289.

Mg II λ 2796.35 Å		Mg II λ 2803.53 Å	
N	v_{rad}	N	v_{rad}
2.9×10^{12}	+15.0	4.5×10^{12}	+15.0
2.6×10^{12}	+7.0	3.8×10^{12}	+7.0
8.0×10^{11}	−0.5	1.2×10^{12}	−0.5
4.6×10^{11}	−4.5	8.5×10^{11}	−5.5
4.5×10^{11}	−26.5	5.0×10^{11}	−29.5
7.3×10^{11}	−43.5	1.0×10^{12}	−38.5

25 000 Å (Bohlin 2007). Rauch et al. (2013) presented a detailed spectral analysis of this star. Based on their model, Rauch et al. (2014a, 2015b, 2014b) identified Zn, Ga, and Ba lines in the observed UV spectrum and determined the abundances of these elements.

We briefly introduce our observational data in Sect. 2. The discovery of the interstellar Mg II $\lambda\lambda$ 2796.35, 2803.53 Å resonance doublet and its modelling is shown in Sect. 3. Our model atmospheres are described in Sect. 4. We start our spectral analysis with a search for Al lines and an abundance determination in Sect. 5. The Zr transition-probability calculation, line identification, and abundance analysis are presented in Sect. 6, followed by the same for Xe in Sect. 7. We summarize our results and conclude in Sect. 8.

2. Observations

For RE 0503−289, we analyzed ultraviolet (UV) observations that were obtained with the Far Ultraviolet Spectroscopic Explorer (FUSE, 910 Å $<\lambda<$ 1188 Å, resolving power $R=\lambda/\Delta\lambda\approx 20\,000$) and the *Hubble* Space Telescope/Space Telescope Imaging Spectrograph (HST/STIS, 1144 Å $<\lambda<$ 3073 Å, $R\approx 45\,800$). These were described in detail by Werner et al. (2012b) and Rauch et al. (2016b), respectively.

For G191−B2B, we used the FUSE observation described by Rauch et al. (2013) and the high-dispersion échelle spectrum (HST/STIS, 1145−3145 Å, $R\approx 100\,000$, Rauch et al. 2013) available from the CALSPEC[1] database.

To compare observations with synthetic spectra, the latter were convolved with Gaussians to model the respective resolving power. The observed spectra are shifted to rest wavelengths according to radial-velocity measurements of $v_{\mathrm{rad}} = 24.56\,\mathrm{km\,s^{-1}}$ (Lemoine et al. 2002) and $25.8\,\mathrm{km\,s^{-1}}$ for G191−B2B and RE 0503−289 (our value), respectively.

3. Interstellar line absorption

Rauch et al. (2016b) found that the interstellar line absorption toward RE 0503−289 has a multi-velocity structure (radial-velocities $-40\,\mathrm{km\,s^{-1}} < v_{\mathrm{rad}} < +18\,\mathrm{km\,s^{-1}}$). In the HST/STIS spectra of RE 0503−289, the interstellar Mg II $\lambda\lambda$ 2796.35, 2803.53 Å resonance lines ($3s\,^2S_{1/2}$–$3p\,^2P^o_{3/2}$ and $3s\,^2S_{1/2}$–$3p\,^2P^o_{1/2}$ with oscillator strengths of 0.608 and 0.303, respectively) are prominent (Fig. 1) and corroborate such a structure. Table 1 displays the parameters that were used to fit the observation.

[1] http://www.stsci.edu/hst/observatory/cdbs/calspec.html

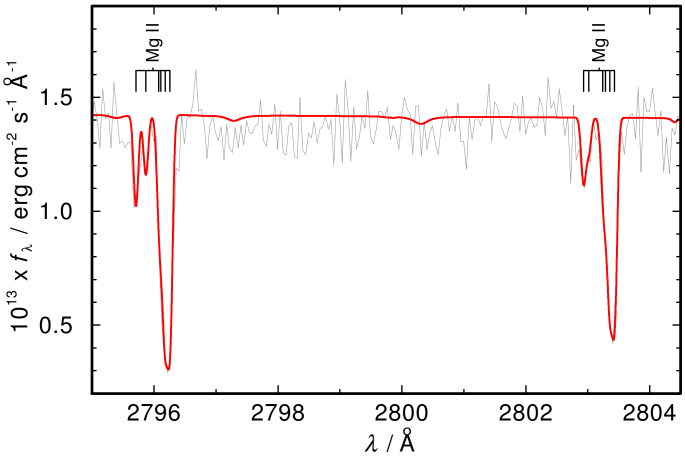

Fig. 1. Section of the STIS spectrum of RE 0503−289 with the interstellar Mg II $\lambda\lambda$ 2796.35, 2803.53 Å lines.

4. Model atmospheres and atomic data

We calculated plane-parallel, chemically homogeneous model-atmospheres in hydrostatic and radiative equilibrium with the Tübingen non-local thermodynamic equilibrium (NLTE) Model Atmosphere Package (TMAP[2], Werner et al. 2003, 2012a). Model atoms were retrieved from the Tübingen Model Atom Database (TMAD[3], Rauch & Deetjen 2003) that has been constructed as part of the Tübingen contribution to the German Astrophysical Virtual Observatory (GAVO[4]).

The effective temperatures, surface gravities, and photospheric abundances of G191−B2B ($T_{\mathrm{eff}} = 60\,000 \pm 2000$ K, $\log(g/\mathrm{cm\,s^{-2}}) = 7.6 \pm 0.05$, Rauch et al. 2013) and RE 0503−289 ($T_{\mathrm{eff}} = 70\,000 \pm 2000$ K, $\log g = 7.50 \pm 0.1$, Rauch et al. 2016b) were previously analyzed with TMAP models. We adopt these parameters for our calculations.

Zr IV–VII and Xe IV–VII were represented by the Zr and Xe model atoms with so-called super levels and super lines that were calculated with a statistical approach via our Iron Opacity and Interface (IrOnIc[5], Rauch & Deetjen 2003; Müller-Ringat 2013). To enable IrOnIc to read our new Zr and Xe data, we transferred it into Kurucz-formatted files (cf., Rauch et al. 2015b). The statistics of our Zr and Xe model atoms is listed in Table 2.

For Zr and Xe and all other species, level dissolution (pressure ionization) following Hummer & Mihalas (1988) and Hubeny et al. (1994) is accounted for. Broadening for all Al, Zr, and Xe lines due to the quadratic Stark effect is calculated using approximate formulae given by Cowley (1970, 1971).

All spectral energy distributions (SEDs) that were calculated for this analysis are available via the registered Theoretical Stellar Spectra Access (TheoSSA[6]) GAVO service.

5. Aluminum in RE 0503−289

The Al abundance in RE 0503−289 was hitherto undetermined. TMAD provides a recently extended Al model atom (Table 3). We used it to search for Al lines in the UV and optical spectra of G191−B2B and RE 0503−289, especially for Al IV lines,

[2] http://astro.uni-tuebingen.de/~TMAP
[3] http://astro.uni-tuebingen.de/~TMAD
[4] http://www.g-vo.org
[5] http://astro.uni-tuebingen.de/~TIRO
[6] http://dc.g-vo.org/theossa

Table 2. Statistics of Zr IV–VII and Xe IV–V, VII atomic levels and line transitions from Tables A.9–A.12 and B.5–B.7, respectively.

Ion	Atomic levels	Lines	Super levels	Super lines
Zr IV	52	135	7	20
Zr V	135	1449	7	22
Zr VI	96	1098	7	12
Zr VII	83	947	7	15
Total	366	3629	28	69
Xe IV	94	1391	7	16
Xe V	65	616	7	15
Xe VI[a]	90	243	7	16
Xe VII	60	491	7	19
Total	309	2741	28	66

Notes. Xe VI is shown for completeness. [(a)] Atomic level and line data taken from Gallardo et al. (2015).

Table 3. Statistics of the Al model atom used in our calculations compared to our previous analyses (e.g., Rauch et al. 2013, 2016b).

Ion	This work		Previous analyses	
	Atomic levels	Lines	Atomic levels	Lines
Al II			1	0
Al III	24	70	7	10
Al IV	61	276	6	3
Al V	43	168	6	4
Al VI	1	0	1	0
	129	514	21	17

because, in both stars, this is the dominant ionization stage in the line-forming region ($-4 \lesssim \log m \lesssim 0.5$, Figs. 2, 3). So far, only Al III lines were identified in the UV spectrum of G191−B2B, namely $\lambda\lambda$1854.714, 1862.787 Å (Holberg et al. 1998) and $\lambda\lambda$1379.668, 1384.130, 1605.764, 1611.812, 1611.854 Å (Rauch et al. 2013, logarithmic mass fraction of Al = −4.95 ± 0.2).

The only additional Al lines found in the observed spectra of G191−B2B are Al III $\lambda\lambda$ 1935.840, 1935.863, and 1935.949 Å (Fig. 4). Al IV lines in our model are entirely too weak to detect them in the observations. Compared to the available STIS spectrum of G191−B2B, that of RE 0503−289 has a much lower signal-to-noise ratio (S/N) that hampers detection of Al lines. Al III $\lambda\lambda$ 1384.130 Å is the only line that is present in the observation and is well reproduced at a solar Al abundance (−4.28±0.2). This result is based on a single line only, and thus it must be judged as uncertain. It is, however, at least an upper abundance limit. The derived abundance is, nonetheless, in good agreement with the expectation (interpolation in Fig. 10). To improve the Al abundance measurement, better UV spectra for RE 0503−289 are highly desirable.

6. Zirconium

6.1. Oscillator-strength calculations for Zr IV–VII ions

Radiative decay rates (oscillator strengths and transition probabilities) were computed using the pseudo-relativistic Hartree-Fock (HFR) method originally introduced by Cowan (1981), and modified for taking into account core-polarization effects

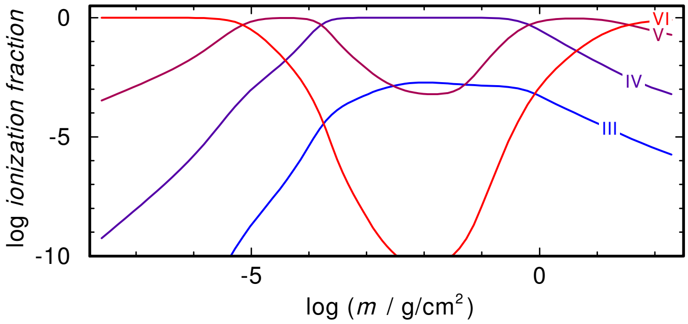

Fig. 2. Al ionization fractions in our G191−B2B model. m is the column mass, measured from the outer boundary of our model atmospheres.

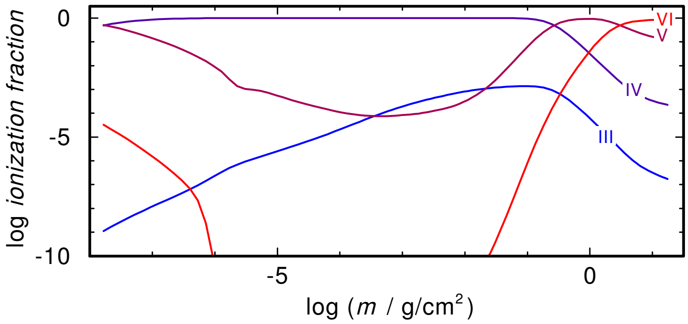

Fig. 3. As Fig. 2, for RE 0503−289.

(CPOL), giving rise to the HFR+CPOL approach (e.g., Quinet et al. 1999, 2002).

For Zr IV, configuration interaction was considered among the configurations $4s^24p^6nd$ (n = 4–9), $4s^24p^6ns$ (n = 5–9), $4s^24p^6ng$ (n = 5–9), $4s^24p^6ni$ (n = 7–9), $4s^24p^54d5p$, $4s^24p^54d4f$, and $4s^24p^54d5f$ for the even parity, and $4s^24p^6np$ (n = 5–9), $4s^24p^6nf$ (n = 4–9), $4s^24p^6nh$ (n = 6–9), $4s^24p^6nk$ (n = 8–9), $4s^24p^54d^2$, $4s^24p^54d5s$, and $4s^24p^54d5d$ for the odd parity. The core-polarization parameters were the dipole polarizability of a Zr VI ionic core as reported by Fraga et al. (1976), that is, α_d = 2.50 a.u., and the cut-off radius corresponding to the HFR mean value $\langle r \rangle$ of the outermost core orbital (4p), that is, r_c = 1.34 a.u. Using the experimental energy levels taken from the analysis by Reader & Acquista (1997), the average energies and spin-orbit parameters of $4s^24p^6nd$ (n = 4–6), $4s^24p^6ns$ (n = 5–8), $4s^24p^6ng$ (n = 5–9), $4s^24p^6np$ (n = 5–7), $4s^24p^6nf$ (n = 4–6), and $4s^24p^66h$ configurations were adjusted using a well-established least-squares fitting procedure in which the mean deviations with experimental data were found to be equal to 0 cm^{-1} for the even parity and 6 cm^{-1} for the odd parity.

For Zr V, the configurations explicitly included in the HFR model were $4s^24p^6$, $4s^24p^5np$ (n = 5–7), $4s^24p^5nf$ (n = 4–7), $4s4p^6nd$ (n = 4–7), $4s4p^6ns$ (n = 5–7), $4s^24p^44d^2$, $4s^24p^44d5s$, and $4s^24p^45s^2$ for the even parity, and $4s^24p^5nd$ (n = 4–7), $4s^24p^5ns$ (n = 5–10), $4s^24p^5ng$ (n = 5–7), $4s4p^6np$ (n = 5–7), $4s4p^6nf$ (n = 4–7), $4s^24p^44d5p$, and $4s^24p^44d4f$ for the odd parity. Core-polarization effects were estimated using α_d = 0.08 a.u. and r_c = 0.45 a.u. These values correspond to a Ni-like Zr XIII ionic core, with 3d as an outermost core subshell. In this ion, the semi-empirical process was performed to optimize the average energies, spin-orbit parameters, and electrostatic interaction. Slater integrals corresponding to $4p^6$, $4p^5np$ (n = 5–6), $4p^54f$, $4s4p^64d$, $4p^5nd$ (n = 4–7), $4p^5ns$ (n = 5–10), $4p^5ng$ (n = 5–6), and $4s4p^65p$ configurations using the experimental levels reported by Reader & Acquista (1979) and

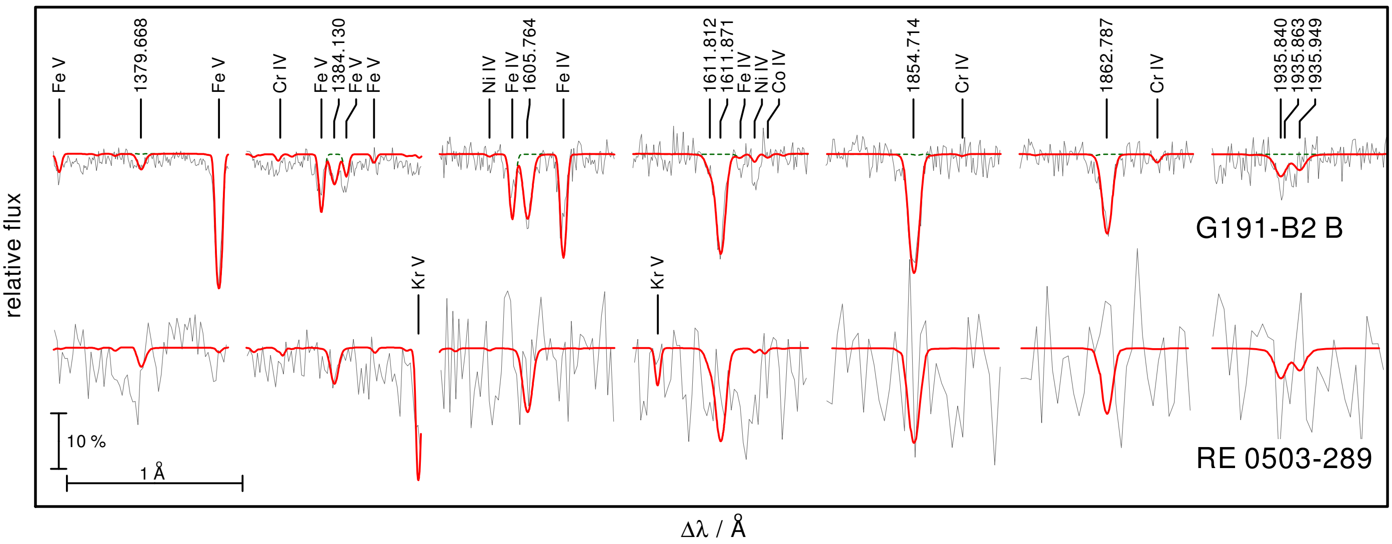

Fig. 4. Comparison of sections of the STIS spectra with our models for G191−B2B (top) and RE 0503−289 (bottom). The Al abundances are 1.1×10^{-5} (0.2 times the solar value, Rauch et al. 2013) and 5.3×10^{-5} (solar), respectively. In the *top part*, the green dashed line is a spectrum calculated without Al. Prominent lines are marked, the identified Al III lines with their wavelengths.

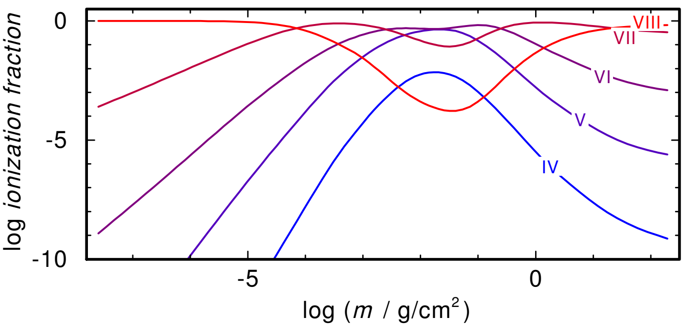

Fig. 5. Like Fig. 2, for Zr.

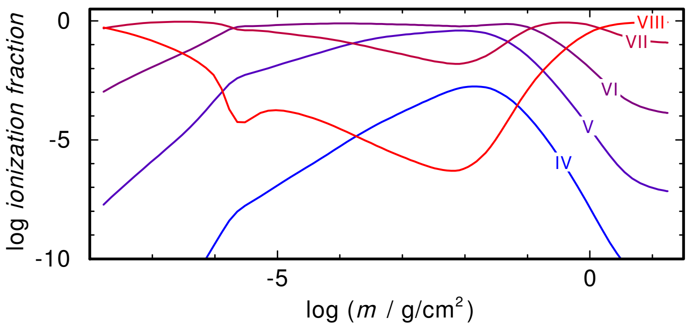

Fig. 6. Like Fig. 3, for Zr.

Khan et al. (1981). The mean deviations between calculated and experimental energies were 77 cm^{-1} and 91 cm^{-1} for even and odd parities, respectively.

In the case of Zr VI, the HFR method was used with the interacting configurations 4s^{2}4p^5, 4s^{2}4p^4*n*p (n = 5–6), 4s^{2}4p^4*n*f (n = 4–6), 4s4p^5*n*d (n = 4–6), 4s4p^5*n*s (n = 5–6), 4p^6*n*p (n = 5–6), 4p^6*n*f (n = 4–6), 4s^{2}4p^{3}4d^2, 4s^{2}4p^{3}4d5s, and 4s^{2}4p^{3}5s^2 for the odd parity, and 4s4p^6, 4s^{2}4p^4*n*d (n = 4–6), 4s^{2}4p^4*n*s (n = 5–6), 4s^{2}4p^4*n*g (n = 5–6), 4s4p^5*n*p (n = 5–6), 4s4p^5*n*f (n = 4–6), 4p^6*n*s (n = 5–6), 4p^6*n*d (n = 4–6), 4s^{2}4p^{3}4d5p, and 4s^{2}4p^{3}4d4f for the even parity. Core-polarization effects were estimated using the same α_d and r_c values as those considered in Zr V. The radial integrals corresponding to 4p^5, 4p^{4}5p, 4s4p^6, 4p^{4}5d, 4p^{4}5s, and 4p^{4}6s were adjusted to minimize the differences between the calculated Hamiltonian eigenvalues and the experimental energy levels taken from Reader & Lindsay (2016). In this process, we found mean deviations equal to 111 cm^{-1} in the odd parity and 221 cm^{-1} in the even parity.

Finally, for Zr VII, the configurations included in the HFR model were 4s^{2}4p^4, 4s^{2}4p^3*n*p (n = 5–6), 4s^{2}4p^3*n*f (n = 4–6), 4s4p^4*n*d (n = 4–6), 4s4p^4*n*s (n = 5–6), 4p^5*n*p (n = 5–6), 4p^5*n*f (n = 4–6), 4s^{2}4p^{2}4d^2, 4s^{2}4p^{2}4d5s, and 4s^{2}4p^{2}5s^2 for the even parity, and 4s4p^5, 4s^{2}4p^3*n*d (n = 4–6), 4s^{2}4p^3*n*s (n = 5–6), 4s^{2}4p^3*n*g (n = 5–6), 4s4p^4*n*p (n = 5–6), 4s4p^4*n*f (n = 4–6), 4p^5*n*s (n = 5–6), 4p^5*n*d (n = 4–6), 4s^{2}4p^{2}4d5p, and 4s^{2}4p^{2}4d4f for the odd parity. The same core-polarization parameters as those used in Zr V and Zr VI calculations were considered while the radial integrals of 4p^4, 4p^{3}5p, 4s4p^5, 4p^{3}4d, and 4p^{3}5s were optimized with the experimental energy levels taken from Reader & Acquista (1976), Rahimullah et al. (1978), Khan et al. (1983). Although having established level values, the 4p^{3}4f configuration was not fitted because it appeared very strongly mixed with experimentally unknown configurations such as 4s4p^{4}4d, and 4s^{2}4p^{2}4d^2 according to our HFR calculations. This semi-empirical process led to mean deviations of 695 cm^{-1} and 479 cm^{-1} for even and odd parities, respectively.

The parameters adopted in our computations are summarized in Tables A.1–A.4 while computed and available experimental energies are compared in Tables A.5–A.8, for Zr IV–VII, respectively. Tables A.9–A.12 give the HFR weighted oscillator strengths (log gf) and transition probabilities (gA, in s^{-1}) together with the numerical values (in cm^{-1}) of the lower and upper energy levels and the corresponding wavelengths (in Å). In the last column of each table, we also give the cancellation factor, CF, as defined by Cowan (1981). We note that very low values of this factor (typically <0.05) indicate strong cancellation effects in the calculation of line strengths. In these cases, the corresponding gf and gA values could be very inaccurate and therefore need to be considered with some care. However, very few of the transitions appearing in Tables A.9–A.12 are affected.

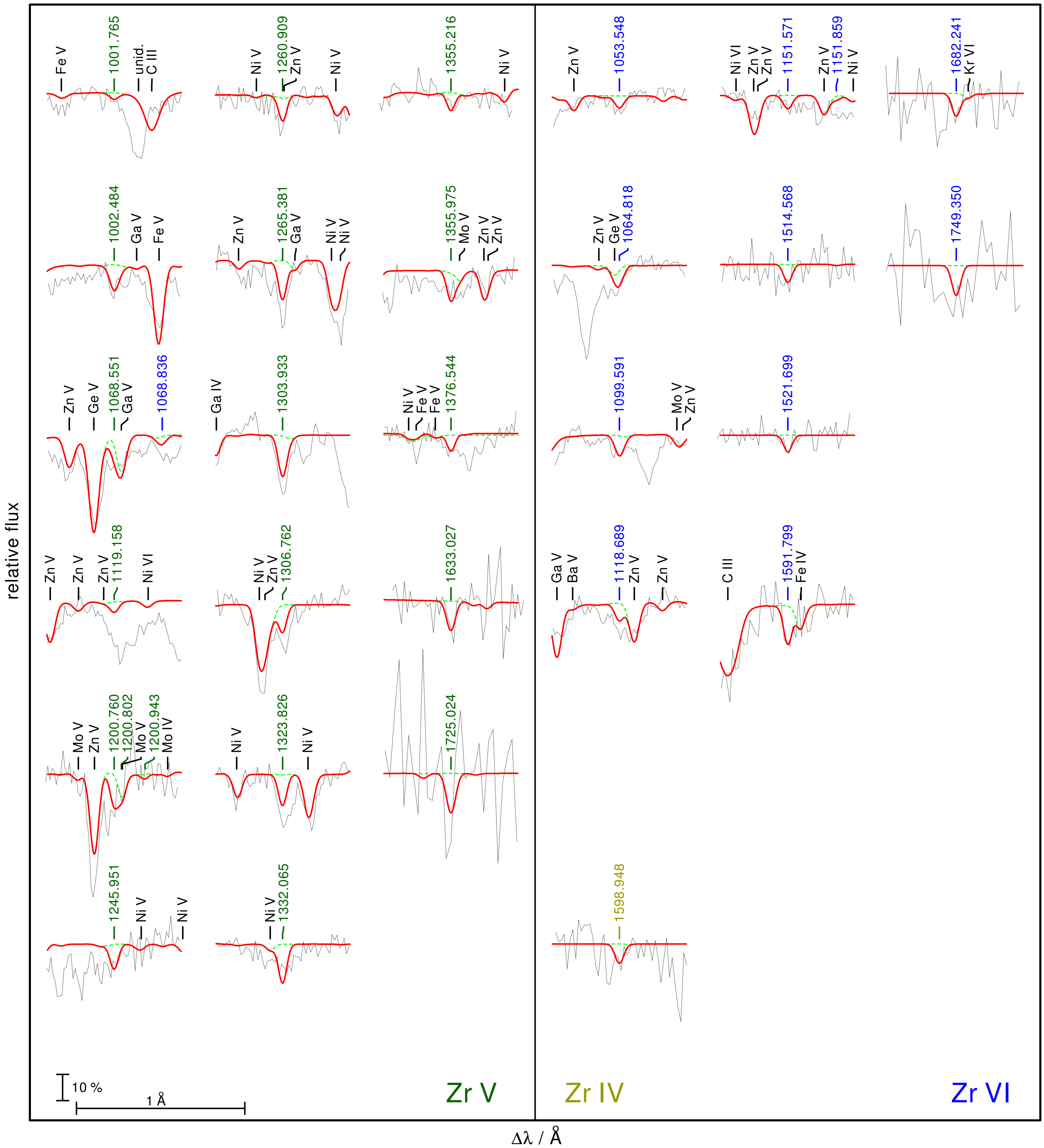

Fig. 7. Identified Zr IV (bottom of *right panel*), Zr V (*left panel*), and Zr VI (*right panel*) lines in the FUSE (λ < 1188 Å) and HST/STIS observations of RE 0503−289. The model (thick, red line) was calculated with an abundance of log Zr = −3.5. The dashed green spectrum was calculated without Zr. Prominent lines are marked, the Zr lines with their wavelengths from Tables A.9–A.11.

These tables are provided via the registered GAVO Tübingen Oscillator Strengths Service (TOSS[7]).

6.2. Zr line identification and abundance analysis

In the FUSE and HST/STIS observations of RE 0503−289, we identified Zr IV–VI lines (Table 4). The observation is well reproduced by our model calculated with a mass fraction of log Zr = −3.5 ± 0.2 (Fig. 7). The Zr IV/V/VI ionization equilibria are matched by our model.

In our synthetic spectra for G191−B2B, Zr IV λ 1598.948 Å is the strongest line. A comparison with the STIS spectrum shows that a Zr mass fraction of 2.6×10^{-6} (approximately 100 times solar, Grevesse et al. 2015) is the upper detection limit (Fig. 8).

[7] http://dc.g-vo.org/TOSS

Table 4. Identified Zr lines in the UV spectrum of RE 0503−289.

		Wavelength/Å	Comment
Zr	IV	1598.948	
Zr	V	1001.765	
		1002.484	
		1068.551	blend Ga V
		1119.158	uncertain
		1200.760	
		1245.951	
		1260.909	
		1265.381	
		1303.933	
		1306.762	
		1323.826	
		1332.065	
		1355.216	
		1355.975	
		1376.544	
		1633.027	
		1725.024	uncertain
Zr	VI	1053.548	
		1064.818	
		1068.663	uncertain
		1099.591	
		1118.689	
		1151.571	
		1514.568	
		1521.699	
		1591.799	
		1682.241	
		1749.350	uncertain

Notes. The wavelengths correspond to those in Tables A.9–A.11.

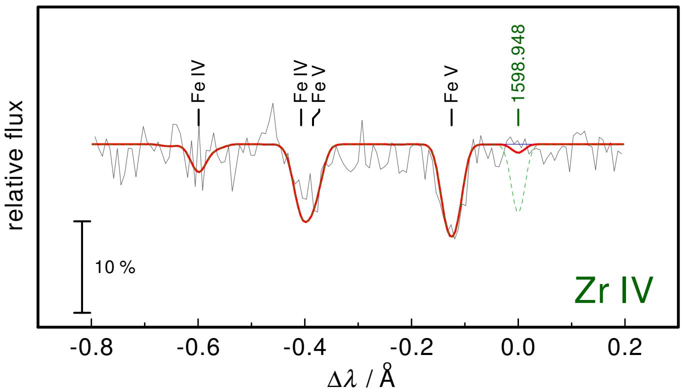

Fig. 8. Section of the STIS spectrum of G191−B2B around Zr IV λ 1598.948 Å compared with three synthetic spectra (thin, blue: no Zr, thick, red: Zr mass fraction = 2.6×10^{-6}, dashed green: Zr = 2.6×10^{-5}).

7. Xenon

7.1. Oscillator-strength calculations for Xe IV, V, and VII ions

New calculations of oscillator strengths and radiative transition probabilities in xenon ions were also performed using the HFR+CPOL method (Cowan 1981; Quinet et al. 1999, 2002).

For Xe IV, the multiconfiguration expansion included $5s^25p^3$, $5s^25p^26p$, $5s^25p^2nf$ (n = 4–6), $5s^25p5d6s$, $5s^25p5d6d$, $5s^25p6s^2$, $5s^25p5d^2$, $5s^25p4f^2$, $5s5p^36s$, $5s5p^3nd$ (n = 5–6), $5s5p^24f5d$, and $5p^5$ for the odd parity, and $5s5p^4$, $5s^25p^2nd$ (n = 5–6), $5s^25p^26s$, $5s^25p^2ng$ (n = 5–6), $5s^25p5d6p$, $5s^25p5dnf$ (n = 4–6), $5s5p^36p$, $5s5p^3nf$ (n = 4–6), and $5s5p^25d^2$ for the even parity. The core-polarization effects were estimated with α_d = 0.88 a.u. and r_c = 0.86 a.u. which correspond to a Pd-like Xe IX ionic core. The former value was taken from Fraga et al. (1976) while the latter one corresponds to the HFR mean value $\langle r \rangle$ of the outermost core orbital (4d). The experimental energy levels published by Saloman (2004) were then used to optimize the radial parameters belonging to the $5p^3$, $5p^26p$, $5p^24f$, $5s5p^4$, $5p^25d$, and $5p^26s$ configurations allowing us to reach average deviations between calculated and observed energies of 137 cm^{-1} and 251 cm^{-1}, for odd and even parities, respectively.

In the case of Xe V, the following sets of configurations were considered in the HFR model: $5s^25p^2$, $5s^25p6p$, $5s^25pnf$ (n = 4–6), $5s^25d6s$, $5s^25d6d$, $5s^26s^2$, $5s^25d^2$, $5s^24f^2$, $5s^25f^2$, $5s5p^26s$, $5s5p^2nd$ (n = 5–6), $5s5p6s6p$, $5s5p6pnd$ (n = 5–6), $5s5p4fnd$ (n = 5–6), $5p^4$, $5p^36p$, and $5p^3nf$ (n = 4–6) for the even parity, and $5s5p^3$, $5s^25pnd$ (n = 5–6), $5s^25pns$ (n = 6–7), $5s^25png$ (n = 5–6), $5s^25d6p$, $5s^25dnf$ (n = 4–6), $5s5p^26p$, $5s5p^2nf$ (n = 4–6), $5s5p6snd$ (n = 5–6), $5s5p5d6d$, $5s5p6s^2$, $5s5p5d^2$, $5p^36s$, and $5p^3nd$ (n = 5–6) for the odd parity. The same core-polarization parameters as those used for Xe IV were used and the experimental energy levels reported by Saloman (2004) and Raineri et al. (2009) were incorporated into the semi-empirical fit to adjust the radial integrals corresponding to the $5p^2$, 5p6p, 5p4f, $5s5p^3$, 5p5d, 5p6d, 5p6s, and 5p7s configurations. In this process, we found mean deviations equal to 144 cm^{-1} in the even parity and 110 cm^{-1} in the odd parity.

For Xe VI, we used the same atomic data as those considered in one of our previous papers (Rauch et al. 2015a). More precisely, the radiative rates were taken from the work of Gallardo et al. (2015) who performed HFR+CPOL calculations including 35 odd-parity and 34 even-parity configurations, that is, $5s^2np$ (n = 5–8), $5s^2nf$ (n = 4–8), $5s^2nh$ (n = 6–8), $5s^28k$, $5p^2np$ (n = 6–8), $5p^2nf$ (n = 4–8), $5p^2nh$ (n = 6–8), $5p^28k$, 5s5p6s, 5s5pnd (n = 5–6), 5s5png (n = 5–6), $5p^3$, 5s5dnf (n = 4–5), 5s6snf (n = 4–5), and $5s5p^2$, $5s^2ns$ (n = 6–8), $5s^2nd$ (n = 5–8), $5s^2ng$ (n = 5–8), $5s^2ni$ (n = 7–8), $5p^2nd$ (n = 5–8), $5p^2ns$ (n = 6–8), $5p^2ng$ (n = 5–8), $5p^2ni$ (n = 7–8), 5s5pnf (n = 4–6), $5s4f^2$, $5s5f^2$, 5s5p6p, $4d^95p^4$, respectively. In this latter study, the core-polarization effects were considered with two different ionic cores, that is, a Cd-like Xe VII core with α_d = 5.80 a.u. for the $5s^2nl$–$5s^2n'l'$ transitions, and a Pd-like Xe IX core with α_d = 0.99 a.u. for all the other transitions. In their semi-empirical least-squares fitting process, Gallardo et al. (2015) achieved standard deviations with experimental energy levels of 149 cm^{-1} in the odd parity and 154 cm^{-1} in the even parity.

Finally, for Xe VII, we used the same model as the one considered by Biémont et al. (2007) extending the set of oscillator strengths to weaker transitions (up to log $gf > -8$). As a reminder, these authors explicitly retained the following configurations in their configuration interaction expansions: $5s^2$, $5p^2$, $5d^2$, $4f^2$, 4fnp (n = 5–6), 4f6f, 4f6h, 5s6s, 5snd (n = 5–6), 5sng (n = 5–6), 5pnf (n = 5–6), 5p6p, 5p6h, 5d6s, 5d6d, and 5dng (n = 5–6) for the even parity, and 5snp (n = 5–6), 5snf (n = 4–6), 5s6h, 4f6s, 4fnd (n = 5–6), 4fng (n = 5–6), 5p6s, 5pnd (n = 5–6), 5png (n = 5–6), 5d6p, and 5dnf (n = 5–6), 5d6h for the odd parity. The same ionic core parameters as those used for Xe IV and Xe V ions were considered and all the experimental energy levels published by Saloman (2004) were included in the semi-empirical optimization of the radial parameters belonging

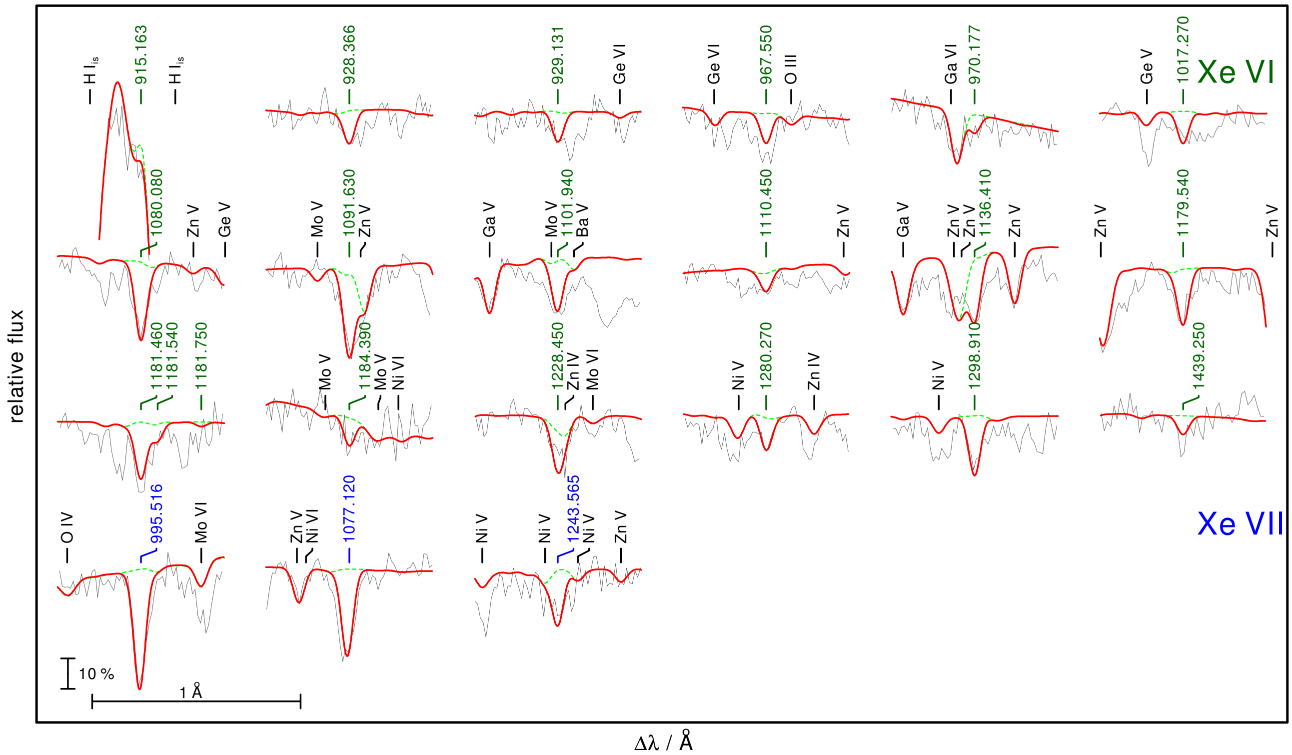

Fig. 9. Identified Xe VI (top three rows) and Xe VII (bottom row) lines in the FUSE ($\lambda < 1188$ Å) and HST/STIS observations of RE 0503−289. The model (thick, red line) was calculated with an abundance of log Xe = −3.9. The dashed, green spectrum was calculated without Xe. Prominent lines are marked ("is" denotes interstellar origin), and the Xe lines are labelled with their wavelengths given by Gallardo et al. (2015) and in Table B.7.

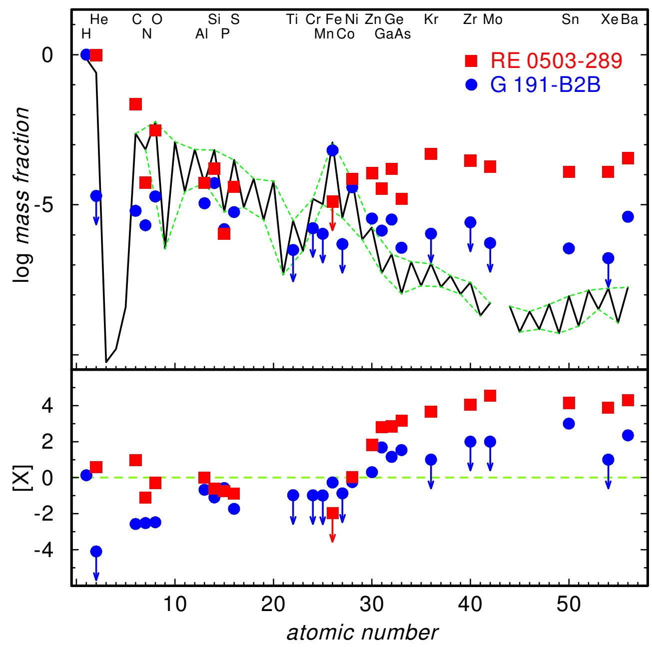

Fig. 10. Solar abundances (Asplund et al. 2009; Scott et al. 2015b,a; Grevesse et al. 2015, thick line; the dashed lines connect the elements with even and with odd atomic number) compared with the determined photospheric abundances of G191−B2B (blue circles, Rauch et al. 2013) and RE 0503−289 (red squares, Dreizler & Werner 1996; Rauch et al. 2012, 2014a,b, 2015a,b, 2016a,b, and this work). The uncertainties of the WD abundances are, in general, approximately 0.2 dex. The arrows indicate upper limits. *Top panel*: abundances given as logarithmic mass fractions. *Bottom panel*: abundance ratios to respective solar values, [X] denotes log (fraction/solar fraction) of species X. The dashed green line indicates solar abundances.

to the 5s^2, 5s6s, 5s5d, 5s6d, 5p^2, 4f5p, 5s5p, 5s6p, 5s4f, 5s5f, 5p6s, and 5p5d configurations giving rise to standard deviations of 377 cm^{-1} and 250 cm^{-1} for even- and odd-parity levels, respectively.

The radial parameters used in our computations are summarized in Tables B.1, B.2 for the Xe IV–V ions, respectively. The calculated energy levels are compared with available experimental values in Tables B.3, B.4 while the HFR weighted oscillator strengths (log gf) and transition probabilities (gA in s^{-1}) are reported in Tables B.5–B.7 for the Xe IV–V and VII ions, respectively. In the latter tables, we also give the numerical values (in cm^{-1}) of lower and upper energy levels of each transition together with the corresponding wavelength (in Å) and the CF, as introduced in Sect. 6.1. These tables are provided via TOSS.

7.2. Xe line identification and abundance analysis

In the FUSE and HST/STIS observations of RE 0503−289, we identified Xe VI-VII lines (Table 5). The observation is well reproduced by our model, calculated with a mass fraction of log Xe = −3.9 ± 0.2 (Fig. 9). This is a factor of two higher than that previously determined by Werner et al. (2012b, log Xe = −4.2 ± 0.6) but agrees within their given error limits. The Xe VI/VII ionization equilibrium is matched by our model.

8. Results and conclusions

To search for Al lines in the observed UV spectrum of RE 0503−289, we created an extended Al model atom for our NLTE model-atmosphere calculations. We could only identify Al III $\lambda\lambda$ 1384.130 Å (Sect. 5), that was well suited to measure the Al abundance. It is reproduced at a solar value (−4.28 ± 0.2, mass

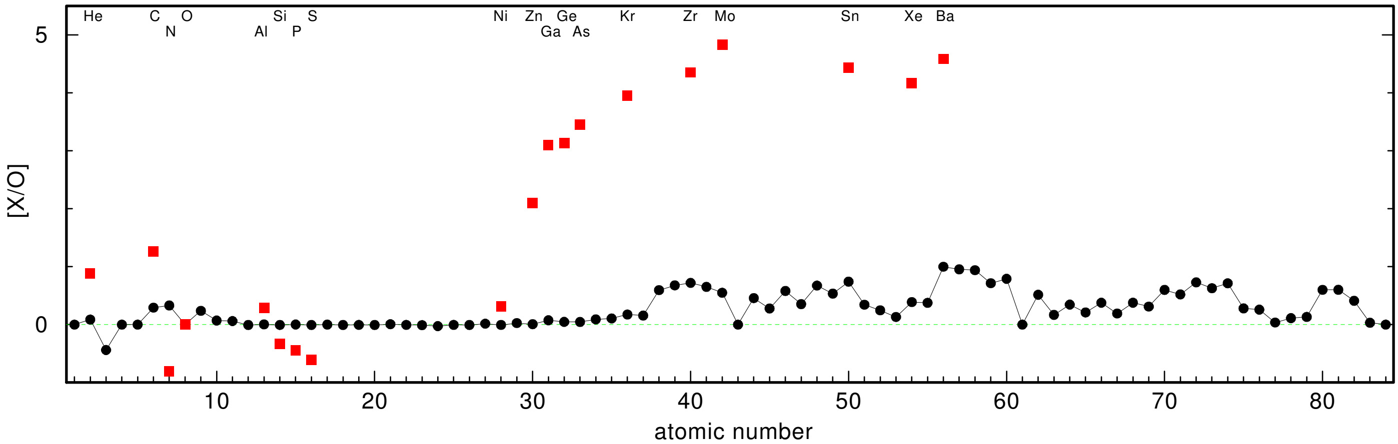

Fig. 11. Determined photospheric abundances of RE 0503−289 (cf. Fig. 10) compared with predictions for surface abundances of Karakas & Lugaro (2016, for an asymptotic giant branch (AGB) star with $M_{\rm initial} = 1.5\,M_\odot$, $M_{\rm final} = 0.585\,M_\odot$, metallicity $Z = 0.014$). [X/O] denotes the normalized log [(fraction of X/solar fraction of X)/(fraction of O/solar fraction of O)] mass ratio. The dashed green line indicates the solar ratio.

Table 5. Identified Xe lines in the UV spectrum of RE 0503−289.

		Wavelength/Å	Comment
Xe	VI	915.163	weak
		928.366[a]	
		929.131[b]	
		967.550[a]	
		970.177	weak
		1017.270[b]	
		1080.080[a]	
		1091.630[a]	
		1101.940[a]	
		1110.450	weak
		1136.410[a]	
		1179.540[a]	
		1181.390[a]	
		1181.540	blend with Xe VI λ 1181.390 Å
		1184.390[a]	uncertain
		1228.450	
		1280.270	
		1298.910[b]	
		1439.250	
Xe	VII	995.516[a]	
		1077.120[a]	
		1243.565	

Notes. The wavelengths correspond to those given in Gallardo et al. (2015) and in Table B.7 for Xe VI and Xe VII, respectively. [(a)] Identified by Werner et al. (2012b); [(b)] identified by Rauch et al. (2015a).

fraction). This needs to be verified once better observations are available.

We identified Zr IV–VI lines in the observed high-resolution UV spectra RE 0503−289 (Table 4). These were well modeled using our newly calculated Zr IV–VII oscillator strengths. We determined a photospheric abundance of log Zr = −3.52 ± 0.2 (mass fraction, 1.5–4.8 × 10^{-4}, 5775–14 480 times the solar abundance). This highly supersolar Zr abundance corresponds to the high abundances of other trans-iron elements in RE 0503−289 (Fig. 10). The Zr IV/V/VI ionization equilibria are well matched by our model ($T_{\rm eff} = 70\,000$ K, $\log g = 7.5$).

In addition to the previously discovered Xe VI–VII lines in the UV spectrum of RE 0503−289, we identified five new Xe VI lines. All identified Xe lines are well matched by our model with an abundance of log Xe = −3.88 ± 0.2 (mass fraction, 0.8–2.1 × 10^{-4}, 4985–12 520 times the solar abundance). This highly supersolar Xe abundance is in line with abundances of other trans-iron elements in RE 0503−289 (Fig. 10).

The amount of trans-iron elements in the photosphere of RE 0503−289 strongly exceeds the yields of nucleosynthesis on the asymptotic giant branch (Fig 11). It is likely that radiative levitation is working efficiently in RE 0503−289 (Rauch et al. 2016a), increasing abundances by up to 4 dex compared with solar values.

The identification of lines of Zr and Xe and their precise abundance determinations only became possible after reliable transition probabilities for Zr IV–VII, Xe IV–V, and Xe VII were computed. Calculations for other, highly-ionized trans-iron elements are necessary to search for their lines and to measure their abundances.

The search for Zr and Xe lines in the UV spectrum of G191−B2B was entirely negative. We established an upper Zr abundance limit of approximately 100 times solar and confirmed the previously found upper limit for Xe of approximately 10 times solar (Rauch et al. 2016a).

Acknowledgements. T.R. and D.H. are supported by the German Aerospace Center (DLR, grants 05 OR 1507 and 50 OR 1501, respectively). The GAVO project had been supported by the Federal Ministry of Education and Research (BMBF) at Tübingen (05 AC 6 VTB, 05 AC 11 VTB) and is funded at Heidelberg (05 AC 11 VH3). Financial support from the Belgian FRS-FNRS is also acknowledged. P.Q. is research director of this organization. Some of the data presented in this paper were obtained from the Mikulski Archive for Space Telescopes (MAST). STScI is operated by the Association of Universities for Research in Astronomy, Inc., under NASA contract NAS5-26555. Support for MAST for non-HST data is provided by the NASA Office of Space Science via grant NNX09AF08G and by other grants and contracts. This research has made use of NASA's Astrophysics Data System and the SIMBAD database, operated at CDS, Strasbourg, France. The TOSS service (`http://dc.g-vo.org/TOSS`) that provides weighted oscillator strengths and transition probabilities was constructed as part of the activities of the German Astrophysical Virtual Observatory.

References

Asplund, M., Grevesse, N., Sauval, A. J., & Scott, P. 2009, ARA&A, 47, 481
Biémont, É., Clar, M., Fivet, V., et al. 2007, Eur. Phys. J. D, 44, 23

Bohlin, R. C. 2007, in The Future of Photometric, Spectrophotometric and Polarimetric Standardization, ed. C. Sterken, ASP Conf. Ser., 364, 315
Cowan, R. D. 1981, in The theory of atomic structure and spectra (Berkeley, CA: University of California Press)
Cowley, C. R. 1970, in The theory of stellar spectra (New York: Gordon & Breach)
Cowley, C. R. 1971, The Observatory, 91, 139
Dreizler, S., & Werner, K. 1996, A&A, 314, 217
Fraga, S., Karwowski, J., & Saxena, K. M. S. 1976, in Handbook of Atomic Data (Amsterdam: Elsevier)
Gallardo, M., Raineri, M., Reyna Almandos, J., Pagan, C. J. B., & Abrahão, R. A. 2015, ApJS, 216, 11
Grevesse, N., Scott, P., Asplund, M., & Sauval, A. J. 2015, A&A, 573, A27
Holberg, J. B., Barstow, M. A., & Sion, E. M. 1998, ApJS, 119, 207
Hubeny, I., Hummer, D. G., & Lanz, T. 1994, A&A, 282, 151
Hummer, D. G., & Mihalas, D. 1988, ApJ, 331, 794
Karakas, A. I., & Lugaro, M. 2016, ApJ, 825, 26
Khan, Z. A., Rahimullah, K., & Chaghtai, M. S. Z. 1981, Phys. Scr., 23, 843
Khan, Z. A., Chaghtai, M. S. Z., & Rahimullah, K. 1983, J. Phys. B: At. Mol. Phys., 16, 1685
Lemoine, M., Vidal-Madjar, A., Hébrard, G., et al. 2002, ApJS, 140, 67
McCook, G. P., & Sion, E. M. 1999a, ApJS, 121, 1
McCook, G. P., & Sion, E. M. 1999b, VizieR Online Data Catalog: III/210
Müller-Ringat, E. 2013, Dissertation, University of Tübingen, Germany, http://www.ivoa.net/documents/SimDM/index.html
Quinet, P., Palmeri, P., Biémont, É., et al. 1999, MNRAS, 307, 934
Quinet, P., Palmeri, P., Biémont, É., et al. 2002, J. Alloys Comp., 344, 255
Rahimullah, K., Chaghtai, M. S. Z., & Khatoon, S. 1978, Physica Scripta, 18, 96
Raineri, M., Gallardo, M., Padilla, S., & Reyna Almandos, J. 2009, J. Phys. B, 42, 205004
Rauch, T., & Deetjen, J. L. 2003, in Stellar Atmosphere Modeling, eds. I. Hubeny, D. Mihalas, & K. Werner, ASP Conf. Ser., 288, 103
Rauch, T., Werner, K., Biémont, É., Quinet, P., & Kruk, J. W. 2012, A&A, 546, A55
Rauch, T., Werner, K., Bohlin, R., & Kruk, J. W. 2013, A&A, 560, A106
Rauch, T., Werner, K., Quinet, P., & Kruk, J. W. 2014a, A&A, 564, A41
Rauch, T., Werner, K., Quinet, P., & Kruk, J. W. 2014b, A&A, 566, A10
Rauch, T., Hoyer, D., Quinet, P., Gallardo, M., & Raineri, M. 2015a, A&A, 577, A88
Rauch, T., Werner, K., Quinet, P., & Kruk, J. W. 2015b, A&A, 577, A6
Rauch, T., Quinet, P., Hoyer, D., et al. 2016a, A&A, 587, A39
Rauch, T., Quinet, P., Hoyer, D., et al. 2016b, A&A, 590, A128
Reader, J., & Acquista, N. 1976, J. Opt. Soc. Am., 66, 896
Reader, J., & Acquista, N. 1979, J. Opt. Soc. Am., 69, 239
Reader, J., & Acquista, N. 1997, J. Opt. Soc. Am. B, 14, 1328
Reader, J., & Lindsay, M. D. 2016, Phys. Scr., 91, 025401
Saloman, E. B. 2004, J. Phys. Chem. Ref. Data, 33, 765
Scott, P., Asplund, M., Grevesse, N., Bergemann, M., & Sauval, A. J. 2015a, A&A, 573, A26
Scott, P., Grevesse, N., Asplund, M., et al. 2015b, A&A, 573, A25
Werner, K., Deetjen, J. L., Dreizler, S., et al. 2003, in Stellar Atmosphere Modeling, eds. I. Hubeny, D. Mihalas, & K. Werner, ASP Conf. Ser., 288, 31
Werner, K., Dreizler, S., & Rauch, T. 2012a, Astrophysics Source Code Library [record ascl:1212.015]
Werner, K., Rauch, T., Ringat, E., & Kruk, J. W. 2012b, ApJ, 753, L7

Appendix A: Additional tables for zirconium

Table A.1. Radial parameters (in cm^{-1}) adopted for the calculations in Zr IV.

Configuration	Parameter	HFR	Fitted	Ratio	Note[a]
		Even parity			
4d	E_{av}	3588	3569		
	ζ_{4d}	515	503	0.975	
5d	E_{av}	149 752	147 800		
	ζ_{5d}	116	136	1.172	
6d	E_{av}	200 505	198 248		
	ζ_{6d}	53	64	1.209	
5s	E_{av}	42 289	41 703		
6s	E_{av}	155 574	152 690		
7s	E_{av}	202 666	200 188		
8s	E_{av}	227 115	224 846		
5g	E_{av}	208 796	207 068		
	ζ_{5g}	0.4	0.4	1.000	F
6g	E_{av}	230 427	228 611		
	ζ_{6g}	0.2	0.2	1.000	F
7g	E_{av}	243 494	241 615		
	ζ_{7g}	0.1	0.1	1.000	F
8g	E_{av}	251 971	250 056		
	ζ_{8g}	0.1	0.1	1.000	F
9g	E_{av}	257 782	255 844		
	ζ_{9g}	0.0	0.0	1.000	F
		Odd parity			
5p	E_{av}	86 720	85 912		
	ζ_{5p}	1388	1661	1.197	
6p	E_{av}	173 349	170 865		
	ζ_{6p}	567	668	1.178	
7p	E_{av}	211 618	209 318		
	ζ_{7p}	290	341	1.174	
4f	E_{av}	162 823	161 581		
	ζ_{4f}	2.3	2.3	1.000	F
5f	E_{av}	205 133	202 889		
	ζ_{5f}	1.3	1.3	1.000	F
6f	E_{av}	228 142	225 772		
	ζ_{6f}	0.8	0.8	1.000	F
6h	E_{av}	230 751	228 744		
	ζ_{6h}	0.1	0.1	1.000	F

Notes. [(a)] F: Fixed parameter value.

Table A.2. Radial parameters (in cm^{-1}) adopted for the calculations in Zr V.

Configuration	Parameter	HFR	Fitted	Ratio	Note[a]
		Even parity			
$4p^6$	E_{av}	17 448	17 850		
$4p^5 5p$	E_{av}	387 307	386 625		
	ζ_{4p}	9939	10 310	1.037	
	ζ_{5p}	1865	2181	1.169	
	$F^2(4p,5p)$	22 698	18 416	0.811	
	$G^0(4p,5p)$	4681	3978	0.850	R1
	$G^2(4p,5p)$	6345	5392	0.850	R1
$4p^5 6p$	E_{av}	502 342	500 684		
	ζ_{4p}	9978	10 094	1.012	
	ζ_{6p}	806	806	1.000	F
	$F^2(4p,6p)$	8810	9530	1.082	
	$G^0(4p,6p)$	1627	1480	0.909	R2
	$G^2(4p,6p)$	2338	2127	0.909	R2
$4p^5 4f$	E_{av}	467 645	466 814		
	ζ_{4p}	9921	10 271	1.035	
	ζ_{4f}	5.6	5.6	1.000	F
	$F^2(4p,4f)$	26 008	22 351	0.859	
	$G^2(4p,4f)$	15 949	15 868	0.995	R3
	$G^4(4p,4f)$	10 543	10 489	0.995	R3
$4s4p^6 4d$	E_{av}	489 915	486 506		
	ζ_{4d}	632	602	0.951	
	$G^2(4s,4d)$	59 108	55 453	0.938	
$4p^5 4f$–$4s4p^6 4d$	$R^1(4s4f;4p4d)$	48 624	41 323	0.850	R4
	$R^2(4s4f;4p4d)$	29 168	24 793	0.850	R4
		Odd parity			
$4p^5 4d$	E_{av}	282 268	268 099		
	ζ_{4p}	9573	9593	1.002	
	ζ_{4d}	616	651	1.057	
	$F^2(4p,4d)$	65 494	57 294	0.875	
	$G^1(4p,4d)$	81 132	66 326	0.818	
	$G^3(4p,4d)$	50 008	44 565	0.891	
$4p^5 5d$	E_{av}	479 226	463 036		
	ζ_{4p}	9933	10 320	1.039	
	ζ_{5d}	163	194	1.185	
	$F^2(4p,5d)$	16 341	13 181	0.807	
	$G^1(4p,5d)$	9999	6618	0.662	
	$G^3(4p,5d)$	7140	6306	0.883	
$4p^5 6d$	E_{av}	551 860	535 375		
	ζ_{4p}	9974	10 464	1.049	
	ζ_{6d}	77	77	1.000	F
	$F^2(4p,6d)$	7018	3966	0.565	R5
	$G^1(4p,6d)$	3816	2156	0.565	R5
	$G^3(4p,6d)$	2854	1613	0.565	R5
$4p^5 7d$	E_{av}	589 057	573 664		
	ζ_{4p}	9989	9989	1.000	F
	ζ_{7d}	43	43	1.000	F
	$F^2(4p,7d)$	3731	2109	0.565	R5
	$G^1(4p,7d)$	1940	1096	0.565	R5
	$G^3(4p,7d)$	1484	839	0.565	R5
$4p^5 5s$	E_{av}	349 759	335 259		
	ζ_{4p}	9867	10 182	1.032	
	$G^1(4p,5s)$	7881	7278	0.923	
$4p^5 6s$	E_{av}	495 108	478 170		

Notes. [a] F: Fixed parameter value; R*n*: ratios of these parameters have been fixed in the fitting process.

Table A.2. continued.

Configuration	Parameter	HFR	Fitted	Ratio	Note[a]
	ζ_{4p}	9959	10 316	1.036	
	G^1(4p,6s)	2433	2132	0.876	
$4p^57s$	E_{av}	558 823	542 240		
	ζ_{4p}	9984	10 360	1.038	
	G^1(4p,7s)	1115	980	0.879	
$4p^58s$	E_{av}	592 851	576 592		
	ζ_{4p}	9994	9994	1.000	F
	G^1(4p,8s)	613	552	0.900	F
$4p^59s$	E_{av}	613 233	596 840		
	ζ_{4p}	9998	9998	1.000	F
	G^1(4p,9s)	375	337	0.900	F
$4p^510s$	E_{av}	626 415	610 078		
	ζ_{4p}	10 001	10 001	1.000	F
	G^1(4p,10s)	247	222	0.900	F
$4p^55g$	E_{av}	558 379	542 891		
	ζ_{4p}	10 004	10 394	1.039	
	ζ_{5g}	0.8	0.8	1.000	F
	F^2(4p,5g)	4855	4142	0.853	R6
	G^3(4p,5g)	392	335	0.853	R6
	G^5(4p,5g)	277	236	0.853	R6
$4p^56g$	E_{av}	592 345	576 588		
	ζ_{4p}	10 004	10 388	1.038	
	ζ_{6g}	0.4	0.4	1.000	F
	F^2(4p,6g)	2776	2436	0.877	R7
	G^3(4p,6g)	358	314	0.877	R7
	G^5(4p,6g)	253	222	0.877	R7
$4s4p^65p$	E_{av}	629 514	612 875		
	ζ_{5p}	1879	1879	1.000	F
	G^1(4s,5p)	6870	6183	0.900	F
$4p^54d$–$4p^55s$	R^2(4p4d;4p5s)	–8924	–5044	0.565	R8
	R^1(4p4d;4p5s)	–1482	–837	0.565	R8

Table A.3. Radial parameters (in cm^{-1}) adopted for the calculations in Zr VI.

Configuration	Parameter	HFR	Fitted	Ratio	Note[a]
		Odd parity			
$4p^5$	E_{av}	22 997	23 322		
	ζ_{4p}	10 007	10 580	1.057	
$4p^4 5p$	E_{av}	461 912	446 765		
	$F^2(4p,4p)$	84 088	79 559	0.946	
	α	0	–651		
	ζ_{4p}	10 577	10 907	1.031	
	ζ_{5p}	2382	2701	1.134	
	$F^2(4p,5p)$	26 052	21 472	0.824	
	$G^0(4p,5p)$	5535	4696	0.848	
	$G^2(4p,5p)$	7459	6664	0.893	
		Even parity			
$4s4p^6$	E_{av}	251 206	224 383		
$4p^4 4d$	E_{av}	289 403	291 464		
	$F^2(4p,4p)$	82 744	78 447	0.948	
	α	0	–450		
	ζ_{4p}	10 187	10 521	1.033	
	ζ_{4d}	721	854	1.184	
	$F^2(4p,4d)$	69 677	62 179	0.892	
	$G^1(4p,4d)$	86 802	72 077	0.831	
	$G^3(4p,4d)$	53 829	45 721	0.849	
$4p^4 5d$	E_{av}	536 543	535 860		
	$F^2(4p,4p)$	84 140	77 928	0.926	
	α	0	–450		F
	ζ_{4p}	10 569	10 891	1.030	
	ζ_{5d}	217	259	1.191	
	$F^2(4p,5d)$	19 555	16 945	0.867	
	$G^1(4p,5d)$	10 870	8250	0.759	R1
	$G^3(4p,5d)$	8037	6100	0.759	R1
$4p^4 5s$	E_{av}	386 802	387 950		
	$F^2(4p,4p)$	83 739	79 833	0.953	
	α	0	–665		
	ζ_{4p}	10 498	10 846	1.033	
	$G^1(4p,5s)$	8725	7618	0.873	
$4p^4 6s$	E_{av}	564 837	564 005		
	$F^2(4p,4p)$	84 213	81 311	0.965	
	α	0	–332		
	ζ_{4p}	10 600	11 164	1.053	
	$G^1(4p,6s)$	2787	2372	0.851	
$4s4p^6$–$4p^4 4d$	$R^1(4p4p;4s4d)$	96 078	72 916	0.759	R2
$4s4p^6$–$4p^4 5d$	$R^1(4p4p;4s5d)$	32 299	24 513	0.759	R2

Notes. [(a)] F: Fixed parameter value; R*n*: ratios of these parameters have been fixed in the fitting process.

Table A.4. Radial parameters (in cm^{-1}) adopted for the calculations in Zr VII.

Configuration	Parameter	HFR	Fitted	Ratio	Note[a]
		Even parity			
$4p^4$	E_{av}	23 653	33 968		
	$F^2(4p,4p)$	84 430	65 839	0.780	
	α	0	646		
	ζ_{4p}	10 658	11 259	1.056	
$4p^3 5p$	E_{av}	516 191	514 481		
	$F^2(4p,4p)$	86 163	82 914	0.962	
	α	0	–537		
	ζ_{4p}	11 232	11 776	1.048	
	ζ_{5p}	2920	2920	1.000	F
	$F^2(4p,5p)$	29 125	29 164	1.001	
	$G^0(4p,5p)$	6338	6086	0.960	
	$G^2(4p,5p)$	8477	5272	0.622	
		Odd parity			
$4s4p^5$	E_{av}	246 126	238 581		
	ζ_{4p}	10 648	11 005	1.034	
	$G^1(4s,4p)$	112 472	98 647	0.877	
$4p^3 4d$	E_{av}	320 698	319 713		
	$F^2(4p,4p)$	84 870	81 614	0.962	
	α	0	–508		
	ζ_{4p}	10 822	11 010	1.017	
	ζ_{4d}	824	795	0.964	
	$F^2(4p,4d)$	73 259	69 858	0.954	
	$G^1(4p,4d)$	91 609	77 513	0.846	
	$G^3(4p,4d)$	57 095	48 489	0.849	
$4p^3 5s$	E_{av}	448 971	447 229		
	$F^2(4p,4p)$	85 823	80 727	0.941	
	α	0	–667		
	ζ_{4p}	11 148	11 790	1.058	
	$G^1(4p,5s)$	9475	8104	0.855	
$4s4p^5$–$4p^3 4d$	$R^1(4p4p;4s4d)$	100 074	78 158	0.781	

Notes. [a] F: Fixed parameter value.

Table A.5. Comparison between available experimental and calculated energy levels in Zr IV.

$E_{\rm exp}$[a]	$E_{\rm calc}$[b]	ΔE	J	Leading components (in %) in LS coupling[c]
				Even parity
0.00	0000	0	1.5	99 4d ^{2}D
1250.70	1251	0	2.5	99 4d ^{2}D
38 258.35	38 258	0	0.5	99 5s ^{2}S
146 652.40	146 652	0	1.5	100 5d ^{2}D
147 002.46	147 002	0	2.5	100 5d ^{2}D
152 513.00	152 513	0	0.5	100 6s ^{2}S
197 765.10	197 765	0	1.5	100 6d ^{2}D
197 930.43	197 930	0	2.5	100 6d ^{2}D
200 123.69	200 124	0	0.5	100 7s ^{2}S
206 864.42	206 863	0	3.5	100 5g ^{2}G
206 864.68	206 866	–1	4.5	100 5g ^{2}G
224 813.48	224 813	0	0.5	100 8s ^{2}S
228 479.86	228 479	0	3.5	100 6g ^{2}G
228 480.08	228 480	0	4.5	100 6g ^{2}G
241 526.36	241 526	0	3.5	100 7g ^{2}G
241 526.52	241 527	0	4.5	100 7g ^{2}G
249 995.33	249 995	0	3.5	100 8g ^{2}G
249 995.44	249 996	0	4.5	100 8g ^{2}G
255 800.20	255 801	–1	3.5	100 9g ^{2}G
255 801.50	255 801	1	4.5	100 9g ^{2}G
				Odd parity
81 976.50	81 976	0	0.5	99 5p ^{2}P
84 461.35	84 461	0	1.5	99 5p ^{2}P
159 066.75	159 041	26	2.5	98 4f ^{2}F
159 086.91	159 112	–25	3.5	98 4f ^{2}F
169 809.71	169 810	0	0.5	100 6p ^{2}P
170 815.11	170 815	0	1.5	100 6p ^{2}P
201 114.14	201 105	9	2.5	97 5f ^{2}F
201 162.65	201 171	–9	3.5	97 5f ^{2}F
208 783.36	208 783	0	0.5	100 7p ^{2}P
209 297.66	209 298	0	1.5	100 7p ^{2}P
224 419.90	224 425	–5	2.5	96 6f ^{2}F
224 488.11	224 483	5	3.5	97 6f ^{2}F
228 743.87	228 744	0	4.5	100 6h ^{2}H
228 743.87	228 744	0	5.5	100 6h ^{2}H

Notes. Energies are given in cm^{-1}. [a] From Reader & Acquista (1997). [b] This work.

Table A.6. Comparison between available experimental and calculated energy levels in Zr V.

E_{exp} [a]	E_{calc} [b]	ΔE	J	Leading components (in %) in LS coupling [c]
		Even parity		
0.00	0	0	0	97 $4p^6\ ^1S$
371 895.16	372 099	–204	1	84 $4p^55p\ ^3S$ + 13 $4p^55p\ ^3P$
376 897.68	376 807	91	2	57 $4p^55p\ ^3D$ + 36 $4p^55p\ ^1D$ + 7 $4p^55p\ ^3P$
378 753.36	378 653	100	3	99 $4p^55p\ ^3D$
380 855.53	380 904	–48	1	46 $4p^55p\ ^1P$ + 30 $4p^55p\ ^3D$ + 20 $4p^55p\ ^3P$
382 985.08	382 952	33	2	67 $4p^55p\ ^3P$ + 30 $4p^55p\ ^1D$
388 852.95	388 865	–12	0	77 $4p^55p\ ^3P$ + 22 $4p^55p\ ^1S$
391 998.41	392 073	–75	1	64 $4p^55p\ ^3D$ + 33 $4p^55p\ ^1P$
395 994.98	395 944	51	2	40 $4p^55p\ ^3D$ + 33 $4p^55p\ ^1D$ + 25 $4p^55p\ ^3P$
396 300.35	396 396	–96	1	64 $4p^55p\ ^3P$ + 19 $4p^55p\ ^1P$ + 11 $4p^55p\ ^3S$
402 688.40	402 529	160	0	76 $4p^55p\ ^1S$ + 22 $4p^55p\ ^3P$
434 714.60	434 703	12	1	55 $4s4p^64d\ ^3D$ + 31 $4p^54f\ ^3D$ + 8 $4p^44d^2\ ^3D$
435 759.10	435 755	4	2	56 $4s4p^64d\ ^3D$ + 29 $4p^54f\ ^3D$ + 8 $4p^44d^2\ ^3D$
437 678.10	437 641	38	3	58 $4s4p^64d\ ^3D$ + 25 $4p^54f\ ^3D$ + 9 $4p^44d^2\ ^3D$
450 133.70	450 156	–22	2	49 $4s4p^64d\ ^1D$ + 19 $4p^44d^2\ ^1D$ + 18 $4p^54f\ ^1D$
453 680.80	453 610	71	5	94 $4p^54f\ ^3G$
454 538.80	454 537	1	4	59 $4p^54f\ ^3G$ + 33 $4p^54f\ ^1G$
457 546.70	457 482	65	3	43 $4p^54f\ ^3G$ + 29 $4p^54f\ ^1F$ + 22 $4p^54f\ ^3F$
458 432.20	458 479	–47	4	54 $4p^54f\ ^3F$ + 31 $4p^54f\ ^1G$ + 8 $4p^54f\ ^3G$
460 476.90	460 554	–77	1	62 $4p^54f\ ^3D$ + 18 $4s4p^64d\ ^3D$ + 10 $4p^44d^2\ ^3D$
460 694.10	460 714	–20	2	42 $4p^54f\ ^3D$ + 27 $4p^54f\ ^3F$ + 14 $4s4p^64d\ ^3D$
460 767.50	460 886	–119	3	28 $4p^54f\ ^3D$ + 27 $4p^54f\ ^3F$ + 21 $4p^54f\ ^1F$
464 015.40	463 932	83	2	32 $4p^54f\ ^3F$ + 31 $4p^54f\ ^1D$ + 15 $4s4p^64d\ ^1D$
470 773.50	470 677	96	3	50 $4p^54f\ ^3G$ + 25 $4p^54f\ ^1F$ + 18 $4p^54f\ ^3F$
471 762.40	471 785	–22	4	37 $4p^54f\ ^3F$ + 30 $4p^54f\ ^1G$ + 26 $4p^54f\ ^3G$
473 715.40	473 766	–51	3	40 $4p^54f\ ^3D$ + 26 $4p^54f\ ^3F$ + 19 $4p^54f\ ^1F$
476 130.20	476 166	–35	2	46 $4p^54f\ ^1D$ + 31 $4p^54f\ ^3F$ + 11 $4p^54f\ ^3D$
491 116.00	491 414	–298	1	78 $4p^56p\ ^3S$ + 16 $4p^56p\ ^3P$
494 472.00	495 996	–1524	1	55 $4p^56p\ ^1P$ + 22 $4p^56p\ ^3P$ + 21 $4p^56p\ ^3D$
494 760.00	494 729	31	3	99 $4p^56p\ ^3D$
495 912.00	494 141	1771	2	52 $4p^56p\ ^3D$ + 41 $4p^56p\ ^1D$ + 6 $4p^56p\ ^3P$
496 428.00	496 722	–294	2	73 $4p^56p\ ^3P$ + 24 $4p^56p\ ^1D$
499 459.00	498 891	568	0	55 $4p^56p\ ^1S$ + 42 $4p^56p\ ^3P$
509 310.00	509 042	268	1	67 $4p^56p\ ^3D$ + 30 $4p^56p\ ^1P$
510 066.00	510 179	–113	1	60 $4p^56p\ ^3P$ + 13 $4p^56p\ ^3S$ + 12 $4p^56p\ ^1P$
510 942.00	511 814	–872	0	57 $4p^56p\ ^3P$ + 38 $4p^56p\ ^1S$
511 263.00	510 586	677	2	45 $4p^56p\ ^3D$ + 33 $4p^56p\ ^1D$ + 21 $4p^56p\ ^3P$
		Odd parity		
241 381.30	241 649	–268	0	99 $4p^54d\ ^3P$
243 560.80	243 779	–218	1	97 $4p^54d\ ^3P$
247 962.30	248 100	–138	2	91 $4p^54d\ ^3P$ + 6 $4p^54d\ ^3D$
251 283.30	250 854	429	4	99 $4p^54d\ ^3F$
253 753.40	253 327	426	3	87 $4p^54d\ ^3F$ + 8 $4p^54d\ ^1F$ + 5 $4p^54d\ ^3D$
257 361.30	257 118	243	2	75 $4p^54d\ ^3F$ + 14 $4p^54d\ ^1D$ + 10 $4p^54d\ ^3D$
265 845.50	266 213	–367	3	65 $4p^54d\ ^3D$ + 35 $4p^54d\ ^1F$
270 560.80	270 736	–176	2	49 $4p^54d\ ^1D$ + 26 $4p^54d\ ^3D$ + 24 $4p^54d\ ^3F$
271 601.60	271 544	57	1	96 $4p^54d\ ^3D$
274 654.60	274 810	–155	2	57 $4p^54d\ ^3D$ + 34 $4p^54d\ ^1D$ + 8 $4p^54d\ ^3P$
277 145.50	276 979	166	3	57 $4p^54d\ ^1F$ + 30 $4p^54d\ ^3D$ + 13 $4p^54d\ ^3F$
325 014.87	325 066	–52	2	99 $4p^55s\ ^3P$
327 616.99	327 532	85	1	38 $4p^55s\ ^1P$ + 34 $4p^55s\ ^3P$ + 25 $4p^54d\ ^1P$
328 940.75	328 971	–30	1	68 $4p^54d\ ^1P$ + 15 $4p^55s\ ^3P$ + 12 $4p^55s\ ^1P$
340 315.49	340 258	57	0	99 $4p^55s\ ^3P$
342 245.65	342 305	–60	1	50 $4p^55s\ ^3P$ + 49 $4p^55s\ ^1P$
452 938.91	452 953	–14	0	99 $4p^55d\ ^3P$

Notes. Energies are given in cm^{-1}. [a] From Reader & Acquista (1979) and Khan et al. (1981). [b] This work. [c] Only the first three components that are larger than 5% are given.

Table A.6. continued.

$E_{\rm exp}$ [a]	$E_{\rm calc}$ [b]	ΔE	J	Leading components (in %) in LS coupling [c]
453 905.60	453 911	–5	1	89 $4p^5 5d\ ^3P$ + 10 $4p^5 5d\ ^3D$
455 444.40	455 398	47	4	99 $4p^5 5d\ ^3F$
455 630.80	455 629	2	2	66 $4p^5 5d\ ^3P$ + 24 $4p^5 5d\ ^3D$ + 9 $4p^5 5d\ ^1D$
455 925.27	455 941	–16	3	60 $4p^5 5d\ ^3F$ + 34 $4p^5 5d\ ^1F$ + 5 $4p^5 5d\ ^3D$
457 613.10	457 595	18	2	44 $4p^5 5d\ ^1D$ + 31 $4p^5 5d\ ^3F$ + 23 $4p^5 5d\ ^3D$
458 523.70	458 496	28	3	66 $4p^5 5d\ ^3D$ + 30 $4p^5 5d\ ^1F$
462 307.40	462 375	–68	1	56 $4p^5 5d\ ^3D$ + 37 $4p^5 5d\ ^1P$
471 306.30	471 306	0	2	66 $4p^5 5d\ ^3F$ + 25 $4p^5 5d\ ^1D$ + 7 $4p^5 5d\ ^3D$
472 015.28	472 047	–31	2	41 $4p^5 5d\ ^3D$ + 28 $4p^5 5d\ ^3P$ + 18 $4p^5 5d\ ^1D$
472 338.00	472 335	3	2	89 $4p^5 6s\ ^3P$
472 520.00	472 529	–9	3	36 $4p^5 5d\ ^3F$ + 35 $4p^5 5d\ ^1F$ + 28 $4p^5 5d\ ^3D$
473 172.70	473 173	–1	1	61 $4p^5 6s\ ^1P$ + 36 $4p^5 6s\ ^3P$
476 477.40	476 432	45	1	56 $4p^5 5d\ ^1P$ + 32 $4p^5 5d\ ^3D$ + 6 $4p^5 5d\ ^3P$
487 746.60	487 747	0	0	100 $4p^5 6s\ ^3P$
488 292.70	488 292	0	1	62 $4p^5 6s\ ^3P$ + 38 $4p^5 6s\ ^1P$
528 422.80	528 711	–288	1	83 $4p^5 6d\ ^3P$ + 15 $4p^5 6d\ ^3D$
529 161.60	529 325	–163	4	100 $4p^5 6d\ ^3F$
529 283.30	529 342	–59	2	54 $4p^5 6d\ ^3P$ + 33 $4p^5 6d\ ^3D$ + 11 $4p^5 6d\ ^1D$
529 299.60	529 363	–63	3	52 $4p^5 6d\ ^3F$ + 44 $4p^5 6d\ ^1F$
530 119.70	529 936	183	2	51 $4p^5 6d\ ^1D$ + 24 $4p^5 6d\ ^3F$ + 23 $4p^5 6d\ ^3D$
530 465.50	530 165	300	3	72 $4p^5 6d\ ^3D$ + 22 $4p^5 6d\ ^1F$ + 5 $4p^5 6d\ ^3F$
531 839.00	531 753	86	1	56 $4p^5 6d\ ^1P$ + 39 $4p^5 6d\ ^3D$
536 682.20	536 674	8	2	100 $4p^5 5g\ ^3F$
536 731.50	536 723	9	3	60 $4p^5 5g\ ^3F$ + 39 $4p^5 5g\ ^1F$
536 763.90	536 761	3	2	100 $4p^5 7s\ ^3P$
536 961.40	536 976	–14	6	100 $4p^5 5g\ ^3H$
536 983.90	536 996	–12	5	53 $4p^5 5g\ ^1H$ + 46 $4p^5 5g\ ^3H$
537 213.40	537 217	–4	1	64 $4p^5 7s\ ^1P$ + 35 $4p^5 7s\ ^3P$
537 501.90	537 499	3	4	46 $4p^5 5g\ ^3F$ + 30 $4p^5 5g\ ^3G$ + 24 $4p^5 5g\ ^1G$
537 539.20	537 528	11	3	54 $4p^5 5g\ ^3G$ + 29 $4p^5 5g\ ^1F$ + 17 $4p^5 5g\ ^3F$
537 806.70	537 807	–1	4	39 $4p^5 5g\ ^1G$ + 31 $4p^5 5g\ ^3G$ + 30 $4p^5 5g\ ^3H$
537 816.50	537 820	–3	5	70 $4p^5 5g\ ^3G$ + 15 $4p^5 5g\ ^3H$ + 14 $4p^5 5g\ ^1H$
546 323.00	546 325	–2	1	46 $4p^5 6d\ ^3D$ + 41 $4p^5 6d\ ^1P$ + 12 $4p^5 6d\ ^3P$
552 258.20	552 265	–7	0	100 $4p^5 7s\ ^3P$
552 521.10	552 515	6	1	64 $4p^5 7s\ ^3P$ + 35 $4p^5 7s\ ^1P$
552 878.20	552 884	–6	4	66 $4p^5 5g\ ^3H$ + 26 $4p^5 5g\ ^1G$ + 5 $4p^5 5g\ ^3G$
552 894.50	552 889	5	4	50 $4p^5 5g\ ^3F$ + 34 $4p^5 5g\ ^3G$ + 11 $4p^5 5g\ ^1G$
552 894.70	552 905	–10	5	38 $4p^5 5g\ ^3H$ + 32 $4p^5 5g\ ^1H$ + 30 $4p^5 5g\ ^3G$
552 933.50	552 923	11	3	46 $4p^5 5g\ ^3G$ + 31 $4p^5 5g\ ^1F$ + 23 $4p^5 5g\ ^3F$
568 040.00	567 226	814	1	74 $4p^5 7d\ ^3P$ + 10 $4p^5 7d\ ^3D$ + 10 $4s4p^6 5p\ ^3P$
570 779.30	570 772	7	2	100 $4p^5 6g\ ^3F$
570 828.20	570 823	5	3	63 $4p^5 6g\ ^3F$ + 37 $4p^5 6g\ ^1F$
570 946.50	570 957	–11	6	100 $4p^5 6g\ ^3H$
570 967.60	570 977	–9	5	53 $4p^5 6g\ ^1H$ + 47 $4p^5 6g\ ^3H$
571 271.70	571 267	4	4	44 $4p^5 6g\ ^3F$ + 31 $4p^5 6g\ ^3G$ + 25 $4p^5 6g\ ^1G$
571 306.30	571 301	5	3	55 $4p^5 6g\ ^3G$ + 31 $4p^5 6g\ ^1F$ + 13 $4p^5 6g\ ^3F$
571 376.00	571 674	–298	1	64 $4p^5 8s\ ^1P$ + 34 $4p^5 8s\ ^3P$
571 443.60	571 444	0	4	40 $4p^5 6g\ ^1G$ + 32 $4p^5 6g\ ^3G$ + 28 $4p^5 6g\ ^3H$
571 452.20	571 454	–2	5	71 $4p^5 6g\ ^3G$ + 14 $4p^5 6g\ ^3H$ + 14 $4p^5 6g\ ^1H$
573 776.00	573 860	–84	1	59 $4s4p^6 5p\ ^3P$ + 19 $4p^4 4d5p\ ^3P$ + 9 $4p^5 7d\ ^3P$
583 420.00	584 144	–724	1	44 $4p^5 7d\ ^3D$ + 37 $4p^5 7d\ ^1P$ + 14 $4p^5 7d\ ^3P$
586 704.90	586 704	0	4	55 $4p^5 6g\ ^3F$ + 22 $4p^5 6g\ ^3G$ + 22 $4p^5 6g\ ^1G$
586 718.20	586 718	0	4	71 $4p^5 6g\ ^3H$ + 15 $4p^5 6g\ ^3G$ + 13 $4p^5 6g\ ^1G$
586 734.50	586 735	–1	5	39 $4p^5 6g\ ^3H$ + 33 $4p^5 6g\ ^1H$ + 28 $4p^5 6g\ ^3G$
586 882.00	586 588	294	1	65 $4p^5 8s\ ^3P$ + 34 $4p^5 8s\ ^1P$
591 916.00	591 916	0	1	66 $4p^5 9s\ ^1P$ + 34 $4p^5 9s\ ^3P$
605 118.00	605 118	0	1	66 $4p^5 10s\ ^1P$ + 34 $4p^5 10s\ ^3P$

Table A.7. Comparison between available experimental and calculated energy levels in Zr VI.

E_{exp} [a]	E_{calc} [b]	ΔE	J	Leading components (in %) in LS coupling [c]
				Odd parity
0.00	0	0	1.5	97 $4p^5$ ^2P
15 602.78	15 603	0	0.5	97 $4p^5$ ^2P
421 257.96	421 364	–106	1.5	62 $4p^4(^3P)5p$ ^4P + 9 $4p^4(^3P)5p$ ^4S + 9 $4p^4(^1D)5p$ ^2P
421 991.19	421 898	93	2.5	68 $4p^4(^3P)5p$ ^4P + 23 $4p^4(^3P)5p$ ^4D
425 678.16	426 017	–339	0.5	23 $4p^4(^3P)5p$ ^2P + 44 $4p^4(^3P)5p$ ^4P + 19 $4p^4(^1D)5p$ ^2P
427 118.65	427 134	–15	2.5	60 $4p^4(^3P)5p$ ^2D + 14 $4p^4(^3P)5p$ ^4P + 13 $4p^4(^3P)5p$ ^4D
427 649.11	427 421	228	3.5	89 $4p^4(^3P)5p$ ^4D + 10 $4p^4(^1D)5p$ ^2F
434 797.76	434 744	53	0.5	39 $4p^4(^3P)5p$ ^4P + 22 $4p^4(^3P)5p$ ^4D + 18 $4p^4(^3P)5p$ ^2P
435 427.69	435 124	304	1.5	33 $4p^4(^3P)5p$ ^4D + 18 $4p^4(^3P)5p$ ^2P + 22 $4p^4(^3P)5p$ ^2D
436 859.11	436 770	89	0.5	60 $4p^4(^3P)5p$ ^4D + 14 $4p^4(^3P)5p$ ^2S + 13 $4p^4(^3P)5p$ ^4P
437 477.01	437 605	–128	1.5	48 $4p^4(^3P)5p$ ^4D + 32 $4p^4(^3P)5p$ ^2P + 10 $4p^4(^1D)5p$ ^2P
440 554.88	440 364	191	2.5	59 $4p^4(^3P)5p$ ^4D + 25 $4p^4(^3P)5p$ ^2D + 13 $4p^4(^3P)5p$ ^4P
442 453.66	442 488	–34	1.5	28 $4p^4(^3P)5p$ ^2D + 24 $4p^4(^3P)5p$ ^4S + 15 $4p^4(^3P)5p$ ^4P
444 340.07	444 700	–360	0.5	67 $4p^4(^3P)5p$ ^2S + 13 $4p^4(^3P)5p$ ^2P + 10 $4p^4(^3P)5p$ ^4D
444 879.34	444 961	–82	1.5	45 $4p^4(^3P)5p$ ^4S + 42 $4p^4(^3P)5p$ ^2D + 5 $4p^4(^3P)5p$ ^4P
449 730.72	449 653	77	2.5	83 $4p^4(^1D)5p$ ^2F + 8 $4p^4(^3P)5p$ ^2D
452 999.87	452 910	90	3.5	88 $4p^4(^1D)5p$ ^2F + 10 $4p^4(^3P)5p$ ^4D
455 878.16	455 971	–92	1.5	57 $4p^4(^1D)5p$ ^2P + 21 $4p^4(^1D)5p$ ^2D + 9 $4p^4(^3P)5p$ ^2P
459 077.64	459 024	54	1.5	70 $4p^4(^1D)5p$ ^2D + 19 $4p^4(^3P)5p$ ^2P + 8 $4p^4(^1D)5p$ ^2P
459 580.77	459 640	–60	2.5	89 $4p^4(^1D)5p$ ^2D
464 724.05	464 719	5	0.5	61 $4p^4(^1D)5p$ ^2P + 34 $4p^4(^3P)5p$ ^2P
482 699.28	482 631	68	0.5	78 $4p^4(^1S)5p$ ^2P + 9 $4p^4(^3P)5p$ ^2P + 7 $4p^4(^3P)5p$ ^4D
484 897.26	484 977	–80	1.5	41 $4p^4(^1S)5p$ ^2P + 29 $4s4p^54d$ ^2D + 8 $4p^4(^1D)4f$ ^2D
				Even parity
191 570.67	191 601	–30	0.5	79 $4s4p^6$ ^2S + 21 $4p^4(^1D)4d$ ^2S
248 940.11	248 835	105	2.5	88 $4p^4(^3P)4d$ ^4D
249 322.89	249 299	24	3.5	90 $4p^4(^3P)4d$ ^4D + 6 $4p^4(^3P)4d$ ^4F
250 017.63	249 918	99	1.5	85 $4p^4(^3P)4d$ ^4D
251 818.70	251 917	–98	0.5	85 $4p^4(^3P)4d$ ^4D + 6 $4p^4(^1D)4d$ ^2P + 5 $4p^4(^3P)4d$ ^2P
261 642.90	261 178	465	4.5	89 $4p^4(^3P)4d$ ^4F + 10 $4p^4(^1D)4d$ ^2G
266 145.41	265 622	523	3.5	65 $4p^4(^3P)4d$ ^4F + 17 $4p^4(^3P)4d$ ^2F + 13 $4p^4(^1D)4d$ ^2G
266 278.49	267 703	–1.425	0.5	43 $4p^4(^1D)4d$ ^2P + 37 $4p^4(^3P)4d$ ^2P + 14 $4p^4(^3P)4d$ ^4D
271 296.05	270 956	340	1.5	60 $4p^4(^3P)4d$ ^4F + 12 $4p^4(^1S)4d$ ^2D + 10 $4p^4(^3P)4d$ ^4P
271 374.36	270 685	689	2.5	92 $4p^4(^3P)4d$ ^4F
272 091.26	272 252	–161	0.5	90 $4p^4(^3P)4d$ ^4P
272 834.44	273 006	–172	1.5	45 $4p^4(^3P)4d$ ^4P + 23 $4p^4(^3P)4d$ ^4F + 18 $4p^4(^1D)4d$ ^2P
274 665.60	274 850	–184	1.5	38 $4p^4(^1D)4d$ ^2D + 23 $4p^4(^3P)4d$ ^2D + 10 $4p^4(^3P)4d$ ^2P
276 491.34	276 497	–6	3.5	42 $4p^4(^3P)4d$ ^2F + 25 $4p^4(^3P)4d$ ^4F + 20 $4p^4(^1D)4d$ ^2G
278 742.23	278 849	–107	2.5	73 $4p^4(^3P)4d$ ^4P + 9 $4p^4(^1S)4d$ ^2D + 7 $4p^4(^3P)4d$ ^2F
279 457.21	280 229	–772	1.5	39 $4p^4(^3P)4d$ ^4P + 24 $4p^4(^1D)4d$ ^2P + 22 $4p^4(^3P)4d$ ^2P
283 112.00	283 096	16	2.5	38 $4p^4(^1S)4d$ ^2D + 20 $4p^4(^3P)4d$ ^2D + 19 $4p^4(^3P)4d$ ^4P
285 967.09	285 408	559	3.5	65 $4p^4(^1D)4d$ ^2G + 23 $4p^4(^3P)4d$ ^2F + 9 $4p^4(^1D)4d$ ^2F
286 411.50	285 745	666	4.5	89 $4p^4(^1D)4d$ ^2G + 10 $4p^4(^3P)4d$ ^4F
287 142.42	287 582	–440	2.5	61 $4p^4(^3P)4d$ ^2F + 20 $4p^4(^1D)4d$ ^2F + 11 $4p^4(^1D)4d$ ^2D
299 608.66	299 907	–298	2.5	76 $4p^4(^1D)4d$ ^2F + 12 $4p^4(^3P)4d$ ^2F + 9 $4p^4(^1D)4d$ ^2D
303 517.22	303 778	–260	3.5	80 $4p^4(^1D)4d$ ^2F + 16 $4p^4(^3P)4d$ ^2F
319 336.18	319 348	–11	1.5	62 $4p^4(^1S)4d$ ^2D + 25 $4p^4(^1D)4d$ ^2D
325 576.82	325 455	121	2.5	72 $4p^4(^1S)4d$ ^2D + 13 $4p^4(^1D)4d$ ^2D + 5 $4p^4(^3P)4d$ ^2F
334 694.92	334 643	52	0.5	70 $4p^4(^1D)4d$ ^2S + 18 $4s4p^6$ ^2S + 5 $4p^4(^1D)4d$ ^2P
339 682.78	339 148	535	1.5	49 $4p^4(^3P)4d$ ^2P + 36 $4p^4(^1D)4d$ ^2P + 7 $4p^4(^1D)4d$ ^2D
343 709.55	344 545	–835	2.5	64 $4p^4(^3P)4d$ ^2D + 22 $4p^4(^1D)4d$ ^2D + 10 $4p^4(^1S)4d$ ^2D
346 345.56	345 413	932	0.5	47 $4p^4(^3P)4d$ ^2P + 41 $4p^4(^1D)4d$ ^2P + 8 $4p^4(^1D)4d$ ^2S
358 168.09	358 487	–319	1.5	56 $4p^4(^3P)4d$ ^2D + 18 $4p^4(^1S)4d$ ^2D + 15 $4p^4(^1D)4d$ ^2D

Notes. Energies are given in cm^{-1}. [(a)] From Reader & Lindsay (2016). [(b)] This work. [(c)] Only the first three components that are larger than 5% are given.

Table A.7. continued.

$E_{\rm exp}{}^a$	$E_{\rm calc}{}^b$	ΔE	J	Leading components (in %) in LS coupling^c
364 827.11	364 808	19	2.5	91 $4p^4(^3P)5s\ ^4P$ + 8 $4p^4(^1D)5s\ ^2D$
369 711.65	369 710	1	1.5	51 $4p^4(^3P)5s\ ^2P$ + 38 $4p^4(^3P)5s\ ^4P$ + 10 $4p^4(^1D)5s\ ^2D$
377 452.05	377 510	–58	0.5	90 $4p^4(^3P)5s\ ^4P$ + 9 $4p^4(^1S)5s\ ^2S$
379 776.65	379 721	55	1.5	60 $4p^4(^3P)5s\ ^4P$ + 36 $4p^4(^3P)5s\ ^2P$
384 781.44	384 805	–23	0.5	93 $4p^4(^3P)5s\ ^2P$ + 5 $4p^4(^1S)5s\ ^2S$
393 555.34	393 558	–3	2.5	91 $4p^4(^1D)5s\ ^2D$ + 7 $4p^4(^3P)5s\ ^4P$
394 195.47	394 194	1	1.5	86 $4p^4(^1D)5s\ ^2D$ + 12 $4p^4(^3P)5s\ ^2P$
423 223.46	423 216	7	0.5	83 $4p^4(^1S)5s\ ^2S$ + 8 $4p^4(^3P)5s\ ^4P$ + 6 $4p^4(^3P)5s\ ^2P$
514 465.31	514 326	140	2.5	71 $4p^4(^3P)5d\ ^4D$ + 10 $4p^4(^3P)5d\ ^4F$ + 9 $4p^4(^3P)5d\ ^4P$
514 487.01	514 344	143	3.5	73 $4p^4(^3P)5d\ ^4D$ + 18 $4p^4(^3P)5d\ ^4F$ + 6 $4p^4(^1D)5d\ ^2F$
515 170.73	515 071	100	1.5	60 $4p^4(^3P)5d\ ^4D$ + 19 $4p^4(^3P)5d\ ^4P$ + 6 $4p^4(^1D)5d\ ^2D$
516 443.48	516 466	–22	0.5	45 $4p^4(^3P)5d\ ^4D$ + 25 $4p^4(^3P)5d\ ^4P$ + 17 $4p^4(^3P)5d\ ^2P$
518 061.55	517 912	150	3.5	64 $4p^4(^3P)5d\ ^2F$ + 23 $4p^4(^3P)5d\ ^4F$ + 11 $4p^4(^1D)5d\ ^2G$
521 740.06	521 926	–186	1.5	38 $4p^4(^3P)5d\ ^4D$ + 34 $4p^4(^3P)5d\ ^2D$ + 12 $4p^4(^3P)5d\ ^2P$
522 035.99	522 139	–103	2.5	39 $4p^4(^3P)5d\ ^2D$ + 25 $4p^4(^3P)5d\ ^2F$ + 15 $4p^4(^3P)5d\ ^4P$
528 357.52	528 376	–19	0.5	50 $4p^4(^3P)5d\ ^4D$ + 31 $4p^4(^3P)5d\ ^2P$ + 9 $4p^4(^1D)5d\ ^2P$
528 976.13	528 735	241	1.5	69 $4p^4(^3P)5d\ ^4F$ + 11 $4p^4(^1S)5d\ ^2D$ + 11 $4p^4(^3P)5d\ ^4D$
529 351.71	529 095	257	2.5	58 $4p^4(^3P)5d\ ^4F$ + 14 $4p^4(^3P)5d\ ^4P$ + 12 $4p^4(^3P)5d\ ^4D$
529 945.22	529 724	222	3.5	54 $4p^4(^3P)5d\ ^4F$ + 23 $4p^4(^3P)5d\ ^2F$ + 21 $4p^4(^3P)5d\ ^4D$
530 538.91	530 420	119	1.5	28 $4p^4(^3P)5d\ ^4P$ + 25 $4p^4(^3P)5d\ ^4D$ + 20 $4p^4(^3P)5d\ ^2D$
532 402.86	532 261	142	2.5	52 $4p^4(^3P)5d\ ^4P$ + 29 $4p^4(^3P)5d\ ^2F$ + 11 $4p^4(^3P)5d\ ^4F$
533 736.95	533 652	85	2.5	44 $4p^4(^3P)5d\ ^2D$ + 39 $4p^4(^3P)5d\ ^2F$
534 552.78	534 821	–268	1.5	64 $4p^4(^3P)5d\ ^2P$ + 15 $4p^4(^3P)5d\ ^2D$ + 8 $4p^4(^1D)5d\ ^2P$
543 295.84	543 372	–77	0.5	79 $4p^4(^1D)5d\ ^2S$ + 10 $4p^4(^3P)5d\ ^4P$ + 9 $4p^4(^1D)5d\ ^2P$
544 423.00	544 411	12	1.5	73 $4p^4(^1D)5d\ ^2P$ + 8 $4p^4(^3P)6s\ ^2P$ + 7 $4p^4(^3P)5d\ ^4P$
545 413.52	545 407	7	2.5	90 $4p^4(^3P)6s\ ^4P$ + 8 $4p^4(^1D)6s\ ^2D$
545 666.07	545 943	–277	2.5	74 $4p^4(^1D)5d\ ^2D$ + 16 $4p^4(^1D)5d\ ^2F$
547 213.94	547 484	–270	2.5	74 $4p^4(^1D)5d\ ^2F$ + 14 $4p^4(^1D)5d\ ^2D$ + 7 $4p^4(^3P)5d\ ^2D$
547 471.92	547 470	2	1.5	63 $4p^4(^3P)6s\ ^2P$ + 20 $4p^4(^3P)6s\ ^4P$ + 8 $4p^4(^1D)6s\ ^2D$
547 791.00	548 110	–319	0.5	66 $4p^4(^1D)5d\ ^2P$ + 23 $4p^4(^3P)5d\ ^2P$ + 7 $4p^4(^1D)5d\ ^2S$
548 805.54	549 467	–661	1.5	78 $4p^4(^1D)5d\ ^2D$ + 18 $4p^4(^3P)5d\ ^2D$
558 208.73	558 215	–6	0.5	86 $4p^4(^3P)6s\ ^4P$ + 12 $4p^4(^1S)6s\ ^2S$
559 356.47	559 344	13	1.5	78 $4p^4(^3P)6s\ ^4P$ + 22 $4p^4(^3P)6s\ ^2P$
561 050.32	561 062	–11	0.5	92 $4p^4(^3P)6s\ ^2P$
573 101.84	572 669	433	2.5	82 $4p^4(^1S)5d\ ^2D$
573 301.14	573 148	153	1.5	79 $4p^4(^1S)5d\ ^2D$ + 6 $4p^4(^3P)5d\ ^4F$
574 494.88	574 600	–105	2.5	92 $4p^4(^1D)6s\ ^2D$ + 8 $4p^4(^3P)6s\ ^4P$
574 889.14	574 785	105	1.5	89 $4p^4(^1D)6s\ ^2D$ + 8 $4p^4(^3P)6s\ ^2P$
602 661.00	602 660	1	0.5	83 $4p^4(^1S)6s\ ^2S$ + 10 $4p^4(^3P)6s\ ^4P$ + 5 $4p^4(^3P)6s\ ^2P$

Table A.8. Comparison between available experimental and calculated energy levels in Zr VII.

E_{exp}[a]	E_{calc}[b]	ΔE	J	Leading components (in %) in LS coupling[c]
				Even parity
0	2	–2	2	89 $4p^4$ ^3P + 9 $4p^4$ ^1D
12 557	12 554	3	0	83 $4p^4$ ^3P + 14 $4p^4$ ^1S
13 549	13 550	–1	1	97 $4p^4$ ^3P
27 176	27 176	0	2	88 $4p^4$ ^1D + 9 $4p^4$ ^3P
56 943	56 943	0	0	84 $4p^4$ ^1S + 14 $4p^4$ ^3P
480 659	480 829	–170	1	53 $4p^3(^4S)5p$ ^3P + 11 $4p^3(^4S)5p$ ^5P + 8 $4p^3(^2D)5p$ ^3P
483 891	484 629	–738	2	61 $4p^3(^4S)5p$ ^3P + 17 $4p^3(^4S)5p$ ^5P + 7 $4p^3(^2D)5p$ ^3P
485 937	484 685	1252	0	84 $4p^3(^4S)5p$ ^3P + 7 $4p^3(^2P)5p$ ^3P + 6 $4p^3(^2D)5p$ ^3P
492 000	494 297	–2297	1	33 $4p^3(^2D)5p$ ^1P + 30 $4p^3(^2D)5p$ ^3D + 12 $4p^3(^4S)5p$ ^3P
498 029	498 816	–787	2	48 $4p^3(^2D)5p$ ^3F + 27 $4p^3(^2D)5p$ ^3D + 11 $4p^3(^2P)5p$ ^3D
501 798	502 258	–460	3	64 $4p^3(^2D)5p$ ^3F + 14 $4p^3(^2D)5p$ ^3D + 12 $4p^3(^2P)5p$ ^3D
504 480	505 161	–681	3	74 $4p^3(^2D)5p$ ^1F + 17 $4p^3(^2D)5p$ ^3D
504 897	503 622	1275	1	41 $4p^3(^2D)5p$ ^3D + 37 $4p^3(^2D)5p$ ^1P + 12 $4p^3(^2P)5p$ ^3D
506 544	502 353	4191	2	51 $4p^3(^2D)5p$ ^3D + 29 $4p^3(^2D)5p$ ^3F + 7 $4p^3(^2P)5p$ ^1D
507 603	508 524	–921	4	75 $4p^3(^2D)5p$ ^3F + 16 $4s4p^44d$ ^1G
507 868	507 908	–40	3	64 $4p^3(^2D)5p$ ^3D + 21 $4p^3(^2D)5p$ ^3F + 10 $4p^3(^2D)5p$ ^1F
512 175	513 167	–992	2	57 $4p^3(^2D)5p$ ^3P + 14 $4p^3(^2P)5p$ ^3P + 10 $4p^3(^4S)5p$ ^3P
515 789	515 584	205	0	80 $4p^3(^2D)5p$ ^3P + 11 $4p^3(^2P)5p$ ^1S
522 993	523 937	–944	1	37 $4p^3(^2P)5p$ ^3D + 9 $4p^3(^2P)5p$ ^1P + 8 $4s4p^44d$ ^3D
524 269	524 312	–43	2	53 $4p^3(^2D)5p$ ^1D + 10 $4p^3(^2D)5p$ ^3P + 6 $4s4p^44d$ ^3D
527 639	528 353	–714	2	44 $4p^3(^2P)5p$ ^3D + 10 $4p^3(^4S)4f$ ^3F + 7 $4s4p^44d$ ^1D
530 030	530 023	7	1	61 $4p^3(^2P)5p$ ^3P + 19 $4p^3(^2P)5p$ ^1P
530 591	531 023	–432	0	85 $4p^3(^2P)5p$ ^3P + 6 $4p^3(^4S)5p$ ^3P + 5 $4p^3(^2P)5p$ ^1S
530 672	530 657	15	1	58 $4p^3(^2P)5p$ ^3S + 21 $4p^3(^2D)5p$ ^3P + 6 $4p^3(^2D)5p$ ^1P
534 485	534 639	–154	3	68 $4p^3(^2P)5p$ ^3D + 9 $4p^3(^2D)5p$ ^3F + 8 $4p^3(^2D)5p$ ^1F
537 188	537 174	14	1	22 $4s4p^44d$ ^3D + 19 $4p^3(^4S)4f$ ^5F + 10 $4s4p^44d$ ^3D
538 927	537 535	1392	2	63 $4p^3(^2P)5p$ ^1D + 11 $4p^3(^2D)5p$ ^1D + 8 $4p^3(^2D)5p$ ^3F
540 660	542 310	–1650	2	33 $4p^3(^2P)5p$ ^3P + 12 $4s4p^44d$ ^3P + 9 $4s4p^44d$ ^3P
542 453	541 036	1417	1	34 $4p^3(^2P)5p$ ^1P + 20 $4p^3(^2P)5p$ ^3P + 10 $4p^3(^2D)5p$ ^3D
556 807	556 867	–60	0	63 $4p^3(^2P)5p$ ^1S + 7 $4p^3(^2D)5p$ ^3P + 5 $4s4p^44d$ ^3P
				Odd parity
192 812	192 785	27	2	86 $4s4p^5$ ^3P + 9 $4p^3(^2D)4d$ ^3P
201 981	202 001	–21	1	83 $4s4p^5$ ^3P + 9 $4p^3(^2D)4d$ ^3P
208 638	208 552	86	0	85 $4s4p^5$ ^3P + 10 $4p^3(^2D)4d$ ^3P
243 704	243 873	–169	1	64 $4s4p^5$ ^1P + 27 $4p^3(^2D)4d$ ^1P
262 683	263 032	–349	0	95 $4p^3(^4S)4d$ ^5D
263 119	263 287	–168	1	96 $4p^3(^4S)4d$ ^5D
263 702	263 263	439	2	92 $4p^3(^4S)4d$ ^5D
264 081	263 321	760	3	89 $4p^3(^4S)4d$ ^5D
264 903	264 332	571	4	93 $4p^3(^4S)4d$ ^5D + 5 $4p^3(^2P)4d$ ^3F
275 418	276 399	–981	2	24 $4p^3(^4S)4d$ ^3D + 23 $4p^3(^2D)4d$ ^3D + 23 $4p^3(^2D)4d$ ^3F
280 850	281 217	–367	3	34 $4p^3(^2D)4d$ ^3D + 31 $4p^3(^4S)4d$ ^3D + 12 $4p^3(^2D)4d$ ^3F
282 419	283 129	–710	1	47 $4p^3(^2D)4d$ ^3D + 45 $4p^3(^4S)4d$ ^3D
285 543	285 392	151	2	48 $4p^3(^2D)4d$ ^3F + 23 $4p^3(^2D)4d$ ^3D + 15 $4p^3(^4S)4d$ ^3D
288 053	287 594	459	3	57 $4p^3(^2D)4d$ ^3F + 14 $4p^3(^2D)4d$ ^3D + 12 $4p^3(^2P)4d$ ^3F
289 300	290 371	–1071	0	93 $4p^3(^2D)4d$ ^1S
291 472	290 767	705	4	62 $4p^3(^2D)4d$ ^3F + 16 $4p^3(^2D)4d$ ^3G + 15 $4p^3(^2P)4d$ ^3F
296 679	296 182	497	3	81 $4p^3(^2D)4d$ ^3G + 12 $4p^3(^2D)4d$ ^3F
298 282	298 336	–54	4	67 $4p^3(^2D)4d$ ^3G + 28 $4p^3(^2D)4d$ ^3F
300 720	300 635	85	5	99 $4p^3(^2D)4d$ ^3G

Notes. Energies are given in cm^{-1}. [(a)] From Reader & Acquista (1976), Rahimullah et al. (1978), and Khan et al. (1983). [(b)] This work. [(c)] Only the first three components that are larger than 5% are given.

Table A.8. continued.

$E_{\rm exp}$[a]	$E_{\rm calc}$[b]	ΔE	J	Leading components (in %) in LS coupling[c]
303 437	303 512	–75	4	84 $4p^3(^2D)4d\ ^1G$ + 7 $4p^3(^2D)4d\ ^3G$
311 985	311 104	881	2	53 $4p^3(^2P)4d\ ^1D$ + 21 $4p^3(^2D)4d\ ^1D$ + 11 $4p^3(^2P)4d\ ^3F$
312 987	313 638	–651	1	51 $4p^3(^2P)4d\ ^3D$ + 32 $4p^3(^2D)4d\ ^3D$ + 12 $4p^3(^4S)4d\ ^3D$
317 400	319 578	–2178	0	63 $4p^3(^2P)4d\ ^3P$ + 27 $4p^3(^2D)4d\ ^3P$ + 6 $4p^3(^2D)4d\ ^1S$
320 989	321 259	–270	2	49 $4p^3(^2P)4d\ ^3D$ + 19 $4p^3(^2D)4d\ ^3D$ + 12 $4p^3(^4S)4d\ ^3D$
322 407	322 588	–181	3	73 $4p^3(^2P)4d\ ^3F$ + 12 $4p^3(^2D)4d\ ^3F$ + 8 $4p^3(^2D)4d\ ^3G$
323 711	324 292	–581	2	55 $4p^3(^2P)4d\ ^3F$ + 23 $4p^3(^2D)4d\ ^3F$ + 6 $4p^3(^2D)4d\ ^3D$
323 870	320 328	3542	1	68 $4p^3(^2P)4d\ ^3P$ + 17 $4p^3(^2D)4d\ ^3P$ + 6 $4p^3(^2D)4d\ ^3S$
324 907	325 653	–746	4	70 $4p^3(^2P)4d\ ^3F$ + 12 $4p^3(^2D)4d\ ^1G$ + 8 $4p^3(^2D)4d\ ^3G$
328 276	328 706	–430	3	37 $4p^3(^2P)4d\ ^3D$ + 31 $4p^3(^2D)4d\ ^3D$ + 11 $4p^3(^2P)4d\ ^1F$
330 126	330 701	–575	2	79 $4p^3(^2P)4d\ ^3P$ + 5 $4p^3(^2P)4d\ ^1D$
342 695	340 697	1998	1	83 $4p^3(^2D)4d\ ^3S$ + 13 $4p^3(^2D)4d\ ^3P$
343 828	344 828	–1000	2	82 $4p^3(^2D)4d\ ^3P$ + 10 $4s4p^5\ ^3P$
345 215	344 686	529	1	42 $4p^3(^2D)4d\ ^1P$ + 23 $4p^3(^2D)4d\ ^3P$ + 20 $4s4p^5\ ^1P$
346 462	345 598	864	3	51 $4p^3(^2P)4d\ ^1F$ + 20 $4p^3(^2D)4d\ ^1F$ + 19 $4p^3(^2P)4d\ ^3D$
352 853	353 419	–566	3	42 $4p^3(^4S)4d\ ^3D$ + 26 $4p^3(^2P)4d\ ^3D$ + 16 $4p^3(^2D)4d\ ^3D$
354 335	354 703	–368	1	35 $4p^3(^2D)4d\ ^3P$ + 23 $4p^3(^2D)4d\ ^1P$ + 19 $4p^3(^2P)4d\ ^3P$
355 650	355 413	237	0	61 $4p^3(^2D)4d\ ^3P$ + 24 $4p^3(^2P)4d\ ^3P$ + 14 $4s4p^5\ ^3P$
360 177	360 333	–156	2	30 $4p^3(^4S)4d\ ^3D$ + 27 $4p^3(^2P)4d\ ^3D$ + 16 $4p^3(^2D)4d\ ^1D$
364 897	364 861	36	1	39 $4p^3(^2P)4d\ ^3D$ + 35 $4p^3(^4S)4d\ ^3D$ + 15 $4p^3(^2D)4d\ ^3D$
371 371	371 578	–207	2	54 $4p^3(^2D)4d\ ^1D$ + 19 $4p^3(^2P)4d\ ^1D$ + 11 $4p^3(^2P)4d\ ^3D$
380 360	380 849	–489	3	59 $4p^3(^2D)4d\ ^1F$ + 31 $4p^3(^2P)4d\ ^1F$
397 987	397 488	499	1	82 $4p^3(^2P)4d\ ^1P$
408 775	408 782	–7	2	91 $4p^3(^4S)5s\ ^5S$ + 7 $4p^3(^2P)5s\ ^3P$
418 375	418 373	2	1	85 $4p^3(^4S)5s\ ^3S$ + 6 $4p^3(^2P)5s\ ^1P$
434 766	434 714	52	2	68 $4p^3(^2D)5s\ ^3D$ + 15 $4p^3(^2P)5s\ ^3P$ + 10 $4p^3(^2D)5s\ ^1D$
434 815	434 803	12	1	79 $4p^3(^2D)5s\ ^3D$ + 9 $4p^3(^4S)5s\ ^3S$ + 6 $4p^3(^2P)5s\ ^1P$
439 534	439 566	–32	3	99 $4p^3(^2D)5s\ ^3D$
443 204	443 228	–24	2	77 $4p^3(^2D)5s\ ^1D$ + 19 $4p^3(^2D)5s\ ^3D$
456 721	456 722	–1	0	98 $4p^3(^2P)5s\ ^3P$
458 043	458 073	–30	1	78 $4p^3(^2P)5s\ ^3P$ + 18 $4p^3(^2P)5s\ ^1P$
466 123	466 108	15	2	73 $4p^3(^2P)5s\ ^3P$ + 11 $4p^3(^2D)5s\ ^1D$ + 11 $4p^3(^2D)5s\ ^3D$
469 225	469 212	13	1	67 $4p^3(^2P)5s\ ^1P$ + 14 $4p^3(^2D)5s\ ^3D$ + 11 $4p^3(^2P)5s\ ^3P$

Appendix B: Additional tables for xenon

Table B.1. Radial parameters (in cm^{-1}) adopted for the calculations in Xe IV.

Configuration	Parameter	HFR	Fitted	Ratio	Note[a]
		Odd parity			
$5p^3$	E_{av}	29 571	29 733		
	$F^2(5p,5p)$	53 594	48 082	0.897	
	α	0	–105		
	ζ_{5p}	8331	9017	1.082	
$5p^26p$	E_{av}	220 434	210 991		
	$F^2(5p,5p)$	55 341	42 311	0.764	
	α	0	–136		
	ζ_{5p}	9030	9306	1.031	
	ζ_{6p}	1957	2359	1.205	
	$F^2(5p,6p)$	16 960	13 633	0.804	
	$G^0(5p,6p)$	3574	2628	0.735	
	$G^2(5p,6p)$	4748	2881	0.608	
$5p^24f$	E_{av}	219 539	210 573		
	$F^2(5p,5p)$	53 413	38 692	0.724	
	α	0	570		
	ζ_{4f}	126	126	1.000	F
	ζ_{5p}	8239	8513	1.033	
	$F^2(5p,4f)$	44 254	38 007	0.859	
	$G^2(5p,4f)$	35 873	31 088	0.867	
	$G^4(5p,4f)$	25 004	18 475	0.739	
		Even parity			
$5s5p^4$	E_{av}	145 882	139 362		
	$F^2(5p,5p)$	53 665	48 881	0.911	
	α	0	–398		
	ζ_{5p}	8332	9009	1.081	
	$G^1(5s,5p)$	70 466	50 020	0.710	
$5p^25d$	E_{av}	171 129	166 438		
	$F^2(5p,5p)$	54 305	36 560	0.673	
	α	0	484		
	ζ_{5p}	8633	9163	1.061	
	ζ_{5d}	488	488	1.000	F
	$F^2(5p,5d)$	40 094	33 282	0.830	
	$G^1(5p,5d)$	45 506	35 398	0.778	
	$G^3(5p,5d)$	28 625	21 026	0.734	
$5p^26s$	E_{av}	188 047	178 843		
	$F^2(5p,5p)$	54 876	42 392	0.772	
	α	0	–251		
	ζ_{5p}	8890	9384	1.056	
	$G^1(5p,5d)$	6038	3450	0.571	
$5s5p^4$–$5p^25d$	$R^1(5p5p;5s5d)$	54 354	42 310	0.778	
$5s5p^4$–$5p^26s$	$R^1(5p5p;5s6s)$	–1248	–1123	0.900	F
$5p^25d$–$5p^26s$	$R^2(5p5d;5p6s)$	–12 911	–8781	0.680	R
	$R^1(5p5d;5p6s)$	–5224	–3553	0.680	R

Notes. [(a)] F: Fixed parameter value; R: ratios of these parameters had been fixed in the fitting process.

Table B.2. Radial parameters (in cm^{-1}) adopted for the calculations in Xe V.

Configuration	Parameter	HFR	Fitted	Ratio	Note[a]
		Even parity			
$5p^2$	E_{av}	28 481	29 415		
	$F^2(5p,5p)$	55 631	50 605	0.910	
	α	0	–111		
	ζ_{5p}	9121	9730	1.067	
5p6p	E_{av}	253 537	252 141		
	ζ_{5p}	9817	8816	0.898	
	ζ_{6p}	2614	2694	1.031	
	$F^2(5p,6p)$	19 855	17 257	0.869	
	$G^0(5p,6p)$	4298	3568	0.830	
	$G^2(5p,6p)$	5684	5510	0.969	
5p4f	E_{av}	216 146	210 715		
	ζ_{4f}	178	178	1.000	F
	ζ_{5p}	8855	9606	1.085	
	$F^2(5p,4f)$	48 109	40 305	0.838	
	$G^2(5p,4f)$	36 992	31 844	0.861	
	$G^4(5p,4f)$	26 416	20 142	0.762	
		Odd parity			
$5s5p^3$	E_{av}	142 485	142 543		
	$F^2(5p,5p)$	55 684	47 870	0.860	
	α	0	100		
	ζ_{5p}	9110	9952	1.092	
	$G^1(5s,5p)$	72 784	55 634	0.764	
5p5d	E_{av}	184 432	183 499		
	ζ_{5p}	9384	10 095	1.076	
	ζ_{5d}	608	863	1.418	
	$F^2(5p,5d)$	43 728	37 678	0.862	
	$G^1(5p,5d)$	50 314	39 579	0.787	
	$G^3(5p,5d)$	31 869	25 524	0.801	
5p6d	E_{av}	307 421	305 556		
	ζ_{5p}	9805	9331	0.952	
	ζ_{6d}	233	233	1.000	F
	$F^2(5p,6d)$	14 535	11 608	0.799	
	$G^1(5p,6d)$	8677	10 765	1.241	
	$G^3(5p,6d)$	6311	7518	1.191	
5p6s	E_{av}	215 033	214 915		
	ζ_{5p}	9664	10 297	1.066	
	$G^1(5p,6s)$	6714	6378	0.950	
5p7s	E_{av}	317 520	308 416		
	ζ_{5p}	9833	10 172	1.034	
	$G^1(5p,7s)$	2108	2015	0.956	
$5s5p^3$–5p5d	$R^1(5p5p;5s5d)$	58 429	46 328	0.793	
$5s5p^3$–5p6s	$R^1(5p5p;5s6s)$	–1254	–1129	0.900	F
5p5d–5p6s	$R^2(5p5d;5p6s)$	–13 325	–12 401	0.931	R
	$R^1(5p5d;5p6s)$	–5408	–5033	0.931	R

Notes. [a] F: Fixed parameter value; R: ratios of these parameters have been fixed in the fitting process.

Table B.3. Comparison between available experimental and calculated energy levels in Xe IV.

E_{exp}[a]	E_{calc}[b]	ΔE	J	Leading components (in %) in LS coupling[c]
				Odd parity
0.0	3	–3	1.5	81 $5p^3\ ^4S$ + 12 $5p^3\ ^2P$
13 267.0	13 248	19	1.5	72 $5p^3\ ^2D$ + 13 $5p^3\ ^2P$ + 11 $5p^3\ ^4S$
17 510.7	17 524	–13	2.5	96 $5p^3\ ^2D$
28 036.4	28 043	–7	0.5	96 $5p^3\ ^2P$
35 649.6	35 644	5	1.5	70 $5p^3\ ^2P$ + 20 $5p^3\ ^2D$ + 5 $5p^3\ ^4S$
180 151.5	180 062	90	2.5	68 $5p^2(^3P)4f\ ^4G$ + 7 $5p^2(^1S)4f\ ^2F$ + 7 $5p^2(^3P)4f\ ^4F$
182 219.1	182 422	–203	3.5	50 $5p^2(^3P)4f\ ^4G$ + 14 $5p^2(^3P)4f\ ^4D$ + 14 $5p^2(^3P)4f\ ^4F$
186 109.1	186 093	16	0.5	48 $5p^2(^3P)6p\ ^4D$ + 19 $5p^2(^3P)6p\ ^2S$ + 11 $5p^2(^3P)6p\ ^2P$
187 532.9	187 312	221	3.5	31 $5p^2(^3P)4f\ ^4G$ + 27 $5p^2(^1D)4f\ ^2G$ + 23 $5p^2(^3P)4f\ ^2G$
188 251.8	187 942	310	4.5	83 $5p^2(^3P)4f\ ^4G$ + 9 $5p^2(^3P)4f\ ^4F$
188 720.6	188 478	243	2.5	52 $5p^2(^3P)4f\ ^2D$ + 19 $5p^2(^3P)4f\ ^4G$ + 11 $5p^2(^3P)4f\ ^4D$
189 842.1	189 879	–37	3.5	54 $5p^2(^3P)4f\ ^4D$ + 18 $5p^2(^3P)4f\ ^2G$ + 15 $5p^2(^1D)4f\ ^2G$
190 792.5	190 927	–135	1.5	38 $5p^2(^3P)6p\ ^4D$ + 14 $5p^2(^3P)6p\ ^4P$ + 12 $5p^2(^3P)6p\ ^2D$
191 858.2	192 042	–184	1.5	43 $5p^2(^3P)4f\ ^4F$ + 16 $5p^2(^3P)4f\ ^4D$ + 14 $5p^2(^3P)4f\ ^2D$
191 978.1	192 079	–101	2.5	54 $5p^2(^3P)4f\ ^4D$ + 18 $5p^2(^3P)4f\ ^2D$ + 14 $5p^2(^3P)4f\ ^4F$
193 860.6	193 915	–54	0.5	47 $5p^2(^3P)6p\ ^2S$ + 36 $5p^2(^3P)6p\ ^4D$ + 13 $5p^2(^3P)6p\ ^4P$
195 784.6	195 729	56	1.5	43 $5p^2(^3P)4f\ ^4D$ + 17 $5p^2(^3P)4f\ ^2D$ + 9 $5p^2(^3P)6p\ ^2D$
196 325.2	196 734	–409	3.5	56 $5p^2(^3P)4f\ ^4F$ + 31 $5p^2(^1D)4f\ ^2F$
196 506.1	196 718	–212	2.5	51 $5p^2(^3P)4f\ ^4F$ + 22 $5p^2(^1D)4f\ ^2F$ + 16 $5p^2(^3P)4f\ ^4D$
196 654.7	196 546	108	0.5	86 $5p^2(^3P)4f\ ^4D$ + 6 $5p^2(^1D)4f\ ^2P$
196 724.9	196 748	–23	1.5	31 $5p^2(^3P)6p\ ^4D$ + 20 $5p^2(^3P)6p\ ^2D$ + 17 $5p^2(^3P)4f\ ^4D$
198 943.1	199 026	–83	2.5	85 $5p^2(^3P)6p\ ^4D$ + 6 $5p^2(^1D)6p\ ^2F$
199 397.0	199 389	8	1.5	33 $5p^2(^3P)4f\ ^2D$ + 21 $5p^2(^3P)4f\ ^4F$ + 17 $5p^2(^3P)6p\ ^4S$
200 486.2	200 403	83	2.5	33 $5p^2(^3P)6p\ ^4P$ + 32 $5p^2(^3P)6p\ ^2D$ + 18 $5p^2(^1D)6p\ ^2D$
200 899.4	200 873	26	0.5	72 $5p^2(^3P)6p\ ^4P$ + 11 $5p^2(^3P)6p\ ^2S$ + 10 $5p^2(^3P)6p\ ^2P$
201 027.6	200 782	245	1.5	29 $5p^2(^3P)6p\ ^4S$ + 21 $5p^2(^3P)6p\ ^2D$ + 16 $5p^2(^3P)4f\ ^2D$
202 076.1	202 067	9	4.5	45 $5p^2(^3P)4f\ ^4F$ + 34 $5p^2(^3P)4f\ ^2G$ + 11 $5p^2(^1D)4f\ ^2H$
202 951.1	203 327	–376	3.5	58 $5p^2(^3P)6p\ ^4D$ + 24 $5p^2(^1D)6p\ ^2F$ + 7 $5p^2(^3P)4f\ ^2F$
204 140.0	203 905	235	1.5	47 $5p^2(^3P)6p\ ^4P$ + 20 $5p^2(^3P)6p\ ^4S$ + 15 $5p^2(^1D)6p\ ^2P$
205 205.0	205 427	–222	2.5	46 $5p^2(^1D)4f\ ^2F$ + 15 $5p^2(^3P)4f\ ^2F$ + 8 $5p^2(^3P)6p\ ^4P$
205 216.7	204 872	345	3.5	25 $5p^2(^3P)4f\ ^2F$ + 19 $5p^2(^3P)4f\ ^2G$ + 14 $5p^2(^3P)6p\ ^4D$
206 061.2	205 962	99	1.5	52 $5p^2(^3P)6p\ ^2P$ + 26 $5p^2(^1D)6p\ ^2D$ + 10 $5p^2(^1D)6p\ ^2P$
206 216.2	206 083	133	4.5	40 $5p^2(^1D)4f\ ^2G$ + 31 $5p^2(^1D)4f\ ^2H$ + 13 $5p^2(^3P)4f\ ^4F$
206 713.1	206 868	–155	3.5	30 $5p^2(^1D)4f\ ^2F$ + 21 $5p^2(^1D)4f\ ^2G$ + 14 $5p^2(^3P)4f\ ^4F$
207 056.6	207 071	–14	2.5	17 $5p^2(^3P)6p\ ^4P$ + 16 $5p^2(^1D)4f\ ^2F$ + 13 $5p^2(^3P)6p\ ^2D$
208 621.1	208 870	–249	2.5	43 $5p^2(^3P)4f\ ^2F$ + 15 $5p^2(^3P)6p\ ^2D$ + 9 $5p^2(^1S)4f\ ^2F$
209 343.7	209 185	158	0.5	68 $5p^2(^3P)6p\ ^2P$ + 13 $5p^2(^3P)6p\ ^2S$ + 7 $5p^2(^3P)6p\ ^4D$
213 735.6	213 529	207	1.5	76 $5p^2(^1D)4f\ ^2D$
215 625.5	215 579	47	2.5	39 $5p^2(^1D)6p\ ^2F$ + 24 $5p^2(^1D)4f\ ^2D$ + 16 $5p^2(^3P)6p\ ^2D$
216 141.0	216 086	55	1.5	35 $5p^2(^1D)6p\ ^2D$ + 24 $5p^2(^1D)6p\ ^2P$ + 7 $5p^2(^3P)6p\ ^4P$
216 910.7	216 873	37	2.5	58 $5p^2(^1D)6p\ ^2D$ + 30 $5p^2(^3P)6p\ ^4P$ + 6 $5p^2(^1D)6p\ ^2F$
217 239.7	217 115	125	3.5	31 $5p^2(^1D)6p\ ^2F$ + 30 $5p^2(^3P)4f\ ^2F$ + 14 $5p^2(^3P)6p\ ^4D$
219 001.7	219 675	–673	2.5	36 $5p^2(^1D)4f\ ^2D$ + 17 $5p^2(^3P)6p\ ^2D$ + 16 $5p^2(^1D)6p\ ^2F$
219 717.3	219 565	152	3.5	41 $5p^2(^1D)6p\ ^2F$ + 30 $5p^2(^3P)4f\ ^2F$ + 12 $5p^2(^3P)6p\ ^4D$
220 081.6	220 085	–4	0.5	82 $5p^2(^1D)6p\ ^2P$ + 7 $5p^2(^3P)6p\ ^2S$
220 789.8	220 565	225	0.5	82 $5p^2(^1D)4f\ ^2P$ + 5 $5p^2(^3P)4f\ ^4D$
224 498.2	224 669	–171	1.5	35 $5p^2(^1D)6p\ ^2P$ + 26 $5p^2(^3P)6p\ ^2P$ + 14 $5p^2(^1D)6p\ ^2D$
228 975.4	228 900	75	3.5	79 $5p^2(^1S)4f\ ^2F$ + 8 $5p^2(^1D)4f\ ^2F$
232 811.4	232 916	–105	0.5	82 $5p^2(^1S)6p\ ^2P$ + 6 $5p^2(^3P)6p\ ^2P$
235 560.7	235 449	112	1.5	83 $5p^2(^1S)6p\ ^2P$

Notes. Energies are given in cm^{-1}. [a] From Saloman (2004). [b] This work. [c] Only the first three components that are larger than 5% are given.

Table B.3. continued.

$E_{\rm exp}{}^{a}$	$E_{\rm calc}{}^{b}$	ΔE	J	Leading components (in %) in LS coupling^{c}
				Even parity
99 663.8	99 384	279	2.5	84 $5s5p^4\ ^4P$ + 9 $5p^2(^3P)5d\ ^4P$
106 923.2	106 996	–72	1.5	83 $5s5p^4\ ^4P$ + 10 $5p^2(^3P)5d\ ^4P$
109 254.4	109 497	–243	0.5	82 $5s5p^4\ ^4P$ + 10 $5p^2(^3P)5d\ ^4P$ + 6 $5s5p^4\ ^2S$
121 928.9	122 134	–205	1.5	56 $5s5p^4\ ^2D$ + 15 $5p^2(^1D)5d\ ^2D$ + 8 $5p^2(^3P)5d\ ^2P$
125 474.7	125 429	46	2.5	69 $5s5p^4\ ^2D$ + 19 $5p^2(^1D)5d\ ^2D$ + 5 $5s5p^4\ ^4P$
133 027.4	132 735	292	1.5	28 $5p^2(^3P)5d\ ^2P$ + 24 $5p^2(^3P)5d\ ^4F$ + 15 $5s5p^4\ ^2D$
134 980.6	135 211	–230	1.5	56 $5p^2(^3P)5d\ ^4F$ + 22 $5p^2(^3P)5d\ ^2P$ + 13 $5s5p^4\ ^2P$
136 495.9	136 607	–111	2.5	63 $5p^2(^3P)5d\ ^4F$ + 22 $5p^2(^3P)5d\ ^4D$
136 796.3	136 825	–29	0.5	42 $5p^2(^3P)5d\ ^2P$ + 24 $5s5p^4\ ^2P$ + 13 $5s5p^4\ ^2S$
141 624.8	141 917	–292	3.5	78 $5p^2(^3P)5d\ ^4F$ + 16 $5p^2(^3P)5d\ ^4D$
141 824.4	141 665	159	2.5	39 $5p^2(^1D)5d\ ^2F$ + 31 $5p^2(^3P)5d\ ^2F$ + 18 $5p^2(^3P)5d\ ^4F$
145 011.2	144 856	155	3.5	34 $5p^2(^1D)5d\ ^2F$ + 32 $5p^2(^3P)5d\ ^4D$ + 17 $5p^2(^3P)5d\ ^2F$
145 105.7	145 173	–67	0.5	74 $5p^2(^3P)5d\ ^4D$ + 13 $5s5p^4\ ^2S$
145 991.1	146 341	–350	4.5	81 $5p^2(^3P)5d\ ^4F$ + 16 $5p^2(^1D)5d\ ^2G$
146 206.5	146 263	–57	1.5	78 $5p^2(^3P)5d\ ^4D$ + 8 $5p^2(^3P)5d\ ^4F$
148 685.0	148 601	84	2.5	54 $5p^2(^3P)5d\ ^4D$ + 12 $5p^2(^3P)5d\ ^4F$ + 12 $5p^2(^3P)5d\ ^2F$
150 737.3	150 659	78	0.5	41 $5s5p^4\ ^2S$ + 22 $5p^2(^3P)5d\ ^2P$ + 14 $5p^2(^1D)5d\ ^2S$
155 863.9	155 893	–29	3.5	42 $5p^2(^3P)5d\ ^4D$ + 20 $5p^2(^3P)5d\ ^2F$ + 18 $5p^2(^1D)5d\ ^2G$
157 205.0	157 289	–84	0.5	69 $5p^2(^3P)6s\ ^4P$ + 18 $5p^2(^3P)6s\ ^2P$ + 10 $5p^2(^1S)6s\ ^2S$
159 642.8	159 380	263	2.5	71 $5p^2(^3P)5d\ ^4P$ + 9 $5p^2(^3P)5d\ ^4D$ + 6 $5s5p^4\ ^4P$
160 665.1	160 696	–31	3.5	66 $5p^2(^1D)5d\ ^2G$ + 23 $5p^2(^1D)5d\ ^2F$ + 7 $5p^2(^3P)5d\ ^4D$
161 434.7	161 471	–36	1.5	59 $5p^2(^3P)5d\ ^4P$ + 15 $5p^2(^1D)5d\ ^2P$ + 7 $5s5p^4\ ^4P$
162 866.5	162 752	115	0.5	63 $5p^2(^3P)5d\ ^4P$ + 13 $5p^2(^1D)5d\ ^2P$ + 7 $5s5p^4\ ^4P$
163 463.1	163 608	–145	4.5	81 $5p^2(^1D)5d\ ^2G$ + 16 $5p^2(^3P)5d\ ^4F$
163 596.7	163 137	459	1.5	32 $5s5p^4\ ^2P$ + 30 $5p^2(^3P)5d\ ^2D$ + 16 $5p^2(^1S)5d\ ^2D$
165 280.0	165 268	12	1.5	18 $5p^2(^1D)5d\ ^2P$ + 17 $5s5p^4\ ^2P$ + 17 $5p^2(^3P)5d\ ^2D$
165 995.3	166 060	–65	1.5	80 $5p^2(^3P)6s\ ^4P$ + 7 $5p^2(^3P)6s\ ^2P$
167 206.4	167 606	–399	0.5	65 $5p^2(^3P)6s\ ^2P$ + 23 $5p^2(^3P)6s\ ^4P$
169 001.5	168 667	335	2.5	54 $5p^2(^3P)5d\ ^2D$ + 15 $5p^2(^3P)5d\ ^2F$ + 11 $5p^2(^1D)5d\ ^2F$
170 490.3	170 444	47	2.5	61 $5p^2(^3P)6s\ ^4P$ + 29 $5p^2(^1D)6s\ ^2D$
172 892.2	172 288	604	0.5	49 $5p^2(^1D)5d\ ^2P$ + 24 $5s5p^4\ ^2P$ + 11 $5p^2(^3P)5d\ ^4P$
173 221.8	172 467	755	1.5	54 $5p^2(^3P)6s\ ^2P$ + 33 $5p^2(^1D)6s\ ^2D$
176 041.9	175 731	311	2.5	27 $5p^2(^1D)5d\ ^2F$ + 20 $5p^2(^3P)5d\ ^2F$ + 16 $5p^2(^1D)5d\ ^2D$
176 122.2	176 020	102	1.5	55 $5p^2(^1D)5d\ ^2D$ + 14 $5s5p^4\ ^2D$ + 12 $5p^2(^1D)5d\ ^2P$
177 923.3	177 771	153	3.5	57 $5p^2(^3P)5d\ ^2F$ + 30 $5p^2(^1D)5d\ ^2F$ + 6 $5p^2(^1D)5d\ ^2G$
177 951.1	178 819	–868	0.5	26 $5p^2(^1D)5d\ ^2P$ + 24 $5p^2(^1D)5d\ ^2S$ + 19 $5s5p^4\ ^2P$
179 000.5	178 344	657	2.5	35 $5p^2(^1D)5d\ ^2D$ + 29 $5p^2(^1S)5d\ ^2D$ + 10 $5p^2(^3P)5d\ ^2D$
182 571.0	184 149	–1578	1.5	33 $5p^2(^1D)6s\ ^2D$ + 21 $5p^2(^1D)5d\ ^2P$ + 13 $5p^2(^3P)5d\ ^2P$
186 048.6	185 632	417	2.5	65 $5p^2(^1D)6s\ ^2D$ + 25 $5p^2(^3P)6s\ ^4P$
187 546.9	187 664	–117	1.5	29 $5p^2(^1D)6s\ ^2D$ + 27 $5p^2(^3P)6s\ ^2P$ + 18 $5p^2(^1D)5d\ ^2P$
188 272.6	188 073	200	0.5	36 $5p^2(^1D)5d\ ^2S$ + 18 $5s5p^4\ ^2S$ + 18 $5s5p^4\ ^2P$
190 030.5	190 017	14	2.5	42 $5p^2(^1S)5d\ ^2D$ + 23 $5p^2(^3P)5d\ ^2D$ + 12 $5p^2(^3P)5d\ ^2F$
190 369.3	190 894	–525	1.5	59 $5p^2(^1S)5d\ ^2D$ + 32 $5p^2(^3P)5d\ ^2D$
202 054.6	202 052	3	0.5	86 $5p^2(^1S)6s\ ^2S$ + 6 $5p^2(^3P)6s\ ^4P$

Table B.4. Comparison between available experimental and calculated energy levels in Xe V.

E_{exp}[a]	E_{calc}[b]	ΔE	J	Leading components (in %) in LS coupling[c]
				Even parity
0.0	–6	6	0	87 $5p^2\ ^3P$ + 10 $5p^2\ ^1S$
9291.8	9290	2	1	97 $5p^2\ ^3P$
14 126.7	14 142	–15	2	66 $5p^2\ ^3P$ + 31 $5p^2\ ^1D$
28 411.2	28 402	9	2	65 $5p^2\ ^1D$ + 31 $5p^2\ ^3P$
44 470.4	44 471	–1	0	86 $5p^2\ ^1S$ + 10 $5p^2\ ^3P$
186 746.7	186 635	111	3	54 $5p4f\ ^3G$ + 37 $5p4f\ ^1F$
189 663.8	189 859	–196	3	44 $5p4f\ ^3F$ + 21 $5p4f\ ^3D$ + 21 $5p4f\ ^1F$
190 644.7	190 745	–101	4	52 $5p4f\ ^3G$ + 36 $5p4f\ ^3F$ + 7 $5p4f\ ^1G$
191 603.5	191 400	204	2	78 $5p4f\ ^3F$ + 11 $5p4f\ ^3D$ + 7 $5p4f\ ^1D$
200 010.2	199 897	113	3	32 $5p4f\ ^1F$ + 32 $5p4f\ ^3G$ + 31 $5p4f\ ^3F$
201 545.2	201 629	–84	4	56 $5p4f\ ^3F$ + 39 $5p4f\ ^3G$
202 281.8	202 341	–59	5	95 $5p4f\ ^3G$
205 758.8	205 942	–183	3	71 $5p4f\ ^3D$ + 18 $5p4f\ ^3F$ + 7 $5p4f\ ^1F$
207 366.7	207 261	106	2	76 $5p4f\ ^3D$ + 15 $5p4f\ ^3F$
209 310.7	209 194	116	1	95 $5p4f\ ^3D$
214 317.7	214 380	–62	4	87 $5p4f\ ^1G$
216 745.6	216 701	44	2	82 $5p4f\ ^1D$ + 8 $5p4f\ ^3D$
228 064.9	228 416	–351	1	62 $5p6p\ ^3D$ + 31 $5p6p\ ^1P$
233 999.3	233 744	255	0	83 $5p6p\ ^3P$ + 10 $5p6p\ ^1S$
234 455.6	234 336	120	1	41 $5p6p\ ^3P$ + 18 $5p6p\ ^1P$ + 17 $5p6p\ ^3D$
235 178.9	235 165	14	2	71 $5p6p\ ^3D$ + 11 $5p6p\ ^1D$ + 11 $5p6p\ ^3P$
243 216.5	243 049	168	1	42 $5p6p\ ^3P$ + 24 $5p6p\ ^1P$ + 12 $5p6p\ ^3D$
244 821.3	244 637	184	2	53 $5p6p\ ^3P$ + 22 $5p6p\ ^3D$ + 16 $5p6p\ ^1D$
246 208.0	245 966	242	3	95 $5p6p\ ^3D$
247 810.4	247 929	–119	1	40 $5p6p\ ^3S$ + 36 $5s5p^25d\ ^5D$ + 6 $5p6p\ ^1P$
250 557.2	251 379	–822	2	63 $5p6p\ ^1D$ + 18 $5p6p\ ^3P$ + 6 $5p4\ ^1D$
259 642.3	259 444	198	0	85 $5p6p\ ^1S$ + 10 $5p6p\ ^3P$
				Odd parity
92 182.8	92 194	–11	2	93 $5s5p^3\ ^5S$ + 6 $5s5p^3\ ^3P$
115 286.3	115 441	–155	1	74 $5s5p^3\ ^3D$ + 10 $5s5p^3\ ^3P$ + 9 $5p5d\ ^3D$
116 097.0	116 138	–41	2	72 $5s5p^3\ ^3D$ + 13 $5s5p^3\ ^3P$ + 8 $5p5d\ ^3D$
119 919.0	119 913	6	3	88 $5s5p^3\ ^3D$ + 9 $5p5d\ ^3D$
133 408.1	133 488	–80	0	90 $5s5p^3\ ^3P$ + 8 $5p5d\ ^3P$
134 575.2	134 507	68	1	75 $5s5p^3\ ^3P$ + 10 $5s5p^3\ ^3D$ + 7 $5p5d\ ^3P$
134 702.7	134 496	206	2	41 $5s5p^3\ ^3P$ + 20 $5s5p^3\ ^1D$ + 12 $5s5p^3\ ^3D$
145 807.0	145 525	282	2	31 $5p5d\ ^1D$ + 28 $5s5p^3\ ^1D$ + 27 $5s5p^3\ ^3P$
155 518.1	155 393	125	1	66 $5s5p^3\ ^3S$ + 24 $5s5p^3\ ^1P$
156 506.8	156 303	204	2	86 $5p5d\ ^3F$ + 8 $5s5p^3\ ^1D$
160 630.4	160 677	–47	3	89 $5p5d\ ^3F$
169 672.6	170 261	–588	1	32 $5s5p^3\ ^1P$ + 20 $5p5d\ ^1P$ + 14 $5s5p^3\ ^3S$
169 799.4	170 055	–255	4	96 $5p5d\ ^3F$
170 987.6	170 919	69	2	45 $5p5d\ ^3P$ + 23 $5p5d\ ^3D$ + 12 $5s5p^3\ ^1D$
173 071.7	173 063	9	1	50 $5p5d\ ^3D$ + 23 $5s5p^3\ ^1P$ + 11 $5s5p^3\ ^3S$
181 004.3	181 097	–93	2	39 $5p5d\ ^3D$ + 30 $5p5d\ ^1D$ + 18 $5s5p^3\ ^1D$
182 167.2	182 145	22	3	75 $5p5d\ ^3D$ + 7 $5s5p^3\ ^3D$ + 6 $5p5d\ ^1F$
183 025.2	182 962	63	0	87 $5p5d\ ^3P$ + 8 $5s5p^3\ ^3P$
184 147.6	184 100	48	1	64 $5p5d\ ^3P$ + 18 $5p5d\ ^3D$ + 7 $5s5p^3\ ^3P$
185 795.0	185 780	15	2	41 $5p5d\ ^3P$ + 22 $5p5d\ ^3D$ + 14 $5p5d\ ^1D$
194 033.1	194 105	–72	0	96 $5p6s\ ^3P$
194 138.0	194 159	–21	3	86 $5p5d\ ^1F$ + 8 $5p5d\ ^3D$

Notes. Energies are given in cm^{-1}. [a] From Saloman (2004) and Raineri et al. (2009). [b] This work. [c] Only the first three components that are larger than 5% are given.

Table B.4. continued.

$E_{\mathrm{exp}}{}^{a}$	$E_{\mathrm{calc}}{}^{b}$	ΔE	J	Leading components (in %) in LS coupling^{c}
194 232.9	194 190	43	1	54 5p6s ^{3}P + 25 5p6s ^{1}P + 12 5p5d ^{1}P
199 959.0	199 730	229	1	55 5p5d ^{1}P + 24 5p6s ^{3}P + 9 5s5p^3 ^{1}P
209 068.9	209 078	–9	2	96 5p6s ^{3}P
213 040.2	213 053	–13	1	71 5p6s ^{1}P + 18 5p6s ^{3}P + 6 5p5d ^{1}P
287 391.0	287 420	–29	2	35 5p6d ^{3}P + 29 5p6d ^{3}D + 18 5p6d ^{1}D
287 696.0	288 003	–307	3	36 5p6d ^{3}F + 31 5s5p^{2}4f ^{3}G + 10 5p6d ^{3}D
288 830.0	288 586	244	1	50 5p6d ^{3}D + 14 5p6d ^{3}P + 13 5p6d ^{1}P
298 053.0	298 054	–1	1	69 5p7s ^{3}P + 29 5p7s ^{1}P
298 739.0	298 717	22	4	91 5p6d ^{3}F
299 596.0	299 417	179	2	53 5p6d ^{1}D + 17 5p6d ^{3}D + 15 5p6d ^{3}F
300 327.0	300 484	–157	3	60 5p6d ^{3}D + 26 5p6d ^{3}F
301 555.0	301 796	–241	1	65 5p6d ^{3}P + 24 5p6d ^{3}D
301 998.0	301 794	204	0	92 5p6d ^{3}P
306 065.0	306 081	–16	1	74 5p6d ^{1}P + 11 5p6d ^{3}D + 7 5p6d ^{3}P
312 956.0	312 959	–3	2	99 5p7s ^{3}P
313 883.0	313 880	3	1	70 5p7s ^{1}P + 29 5p7s ^{3}P